Nanoscale surface modification of wood veneers for adhesion

Yu Zhou

Thesis submitted to the Faculty of Virginia Polytechnic Institute and State University in partial fulfillment of the requirements for the degree of

Master of Science

In

Forest Products

Scott Renneckar, Chair

Charles E. Frazier

Maren Roman

September 1, 2008

Blacksburg, Virginia

Keywords: nano, layer-by-layer, wood, coating

Nanoscale surface modification of wood veneers for adhesion

Yu Zhou

ABSTRACT

Surface chemistry of wood is based on the exposed cut surface that is the combination of intact (lumen wall) and cut cell wall material. It is inherently complex and changes with history of processing. Modification of wood surface through noncovalent attachment of amine containing water soluble polyelectrolytes provides a path to create functional surfaces in a controlled manner. Furthermore, modification of the surface can be performed using layer-by-layer (LbL) assembly, where the adsorption of polyelectrolytes or nanoparticles in sequential steps yields a multilayer film with a defined layer sequence on a given substrate. The objective of this study was to quantify adsorption of polyelectrolytes onto wood surface and use these polyelectrolytes as adhesives. In this study, optimal pH conditions for modifying wood surfaces, by anchoring adsorbing polyelectrolytes, were detected using zeta- (ξ)-potential measurements. Positively charged wood surfaces were also detected by the same technique after a layer of poly(diallyldimethylammonium chloride) (PDDA) or poly (ethylenimine) (PEI) was adsorbed. Both X-ray photoelectron spectroscopy (XPS) and Carbon-Nitrogen-Sulfur analyzer (CNS) were used to quantify the amount of charged polymer on wood surfaces to elucidate optimal pH and ionic strength for polyelectrolyte adsorption. Confocal laser scanning microscopy (CLSM) and Environmental Scanning Electron Microscope (ESEM) were used to characterize adsorbed LbL multilayers of poly(acrylic) acid (PAA) and poly(allylamine hydrochloride) (PAH). Cross-linking between PAA and PAH at various temperatures was studied by Fourier Transform Infrared Spectroscopy (FTIR) and the evaluation of multilayer as bonding agents was carried out by compression shear test following ASTM D905 standard.

ACKNOWLEDGEMENTS

I would like to start my sincere appreciation to my major advisor, Dr. Scott Renneckar, who has given me the support, encouragement, guidance and patience during my graduate work. I would have more scrambling and struggling during my graduate study without his advices for all these times. My thanks are also given to my two other committee members, Dr. Charles E. Frazier Dr. Maren Roman for their helpful advices and technique supports.

Thanks are also given to the members of my group, QingQing Li, Zhiyuan Lin, Karthik Pillai, Rob Haupt, and W. Travis Church, and also group members of Dr. Charles E. Frazier, Dr. Maren Roman, and Dr.Zink-Sharp's. I deeply appreciate the friendship we have built during my study here and the kindest help they have offered.

The appreciations are extended to the technical staffs working at the Forest Products Brooks Center—Rick Caudill and David Jones—for their warmly help in technical problems. And I would also like to thank Linda Caudill and Angie Riegel for their assistance in the daily life issues and advices.

I also thank William Clayton Miles in the Department of Chemical Engineering, Jerry Hunter and Stephen McCartney in the Institute for Critical Technology and Applied Science, David O Mitchem in the Department of Forestry, Kristi R. DeCourcy in Fralin Biotechnology Center and Frank from the department of Chemistry for their technical assistance in manipulation of equipments.

Finally, I want to give my greatest thanks to my parents, who have been always educating me to be a useful person, always giving me the warmest care, always offering me the most unselfish support, always being proud of me and always hiding their deeply misses of their dearest daughter to let her focus on the study.

CONTENTS

LIST OF FIGURES

LIST OF TABLES

CHAPTER 1 – INTRODUCTION

1.1 Problem statement

Wood composites have been widely developed because of their positive impact on the environment by reducing the consumption of large diameter timbers and utilizing waste fiber. These materials can have comparable strength with and even better physical properties than solid wood, by having the ability to control their uniformity. In addition to wood and wood by-products, many other materials, like thermoplastics, concrete and metals have been combined to create wood composites with combination of desired properties from each material. However, due to the heterogeneous nature of wood and its lack of dimensional stability when exposed to moisture, improvement in bonding performance has been investigated in detail. Research has been done to improve the adhesion properties in wood composites by adding coupling agents or applying chemical treatments to wood surfaces. In this study, a novel surface modification for wood is investigated to make wood surface more chemically uniform.

Recent studies on layer-by-layer (LbL) assembly of multilayer films show great potentials for surface modification that it is able to add unique properties to a variety of materials by the adsorption of polyelectrolytes or nanoparticles on the surface of materials. This LbL assembly technique has the advantages of its simple proceedings, feasibility to diverse types of adsorbing materials and availability for any size and morphology of the substrate. LbL has been used for the preparation of many types of materials or surface modification including nano-patterning flexible substrates, ultrathin ion-separation membranes, conducting or lighting materials, electrode surface modification, and fiber modification for paper strength. Encouraged by these accomplishments, and especially, the successes of applying LBL in the field of paper science, LbL technique is considered a method for wood surface modification.

Before the application of LbL technique to wood surface, it should be noted that wood is different from any other materials, such as metals and synthetic plastics. Wood is composed by different chemical units, which contain cellulose, hemicelluloses, lignin and extractives. These materials may have varying degree of interaction with the

polyelectrolytes in LbL films. Also, wood has heterogeneous surface properties, such as the cellular structure containing microscale structures of cut cell walls on tangential sections that may affect the outcome of coating, especially the coating of first layer. When wood is cut, it changes access to the polymeric components that make up the surface of wood. Therefore, those factors need to be considered when studying polyelectrolytes adsorption to wood surfaces. Besides the influence from native wood surfaces, two other factors, pH and salt content in the polyelectrolyte solutions, which have been largely studied in LbL area, should be taken into account because they influence polyelectrolyte and surface charges and screening lengths, respectively.

1.2 Objectives

The general scope of this project is to investigate the LbL assembly of multilayer films onto veneer-based wood substrates to serve as adhesive layers. Arising from the results of previous LbL studies from other researchers and combined with the unique properties of wood, there are four objectives below to complete the understanding of multilayers on wood:

1. Quantify the effect of solution parameters on the adsorption of polycations onto wood surfaces.
2. Determine how wood anatomy affects the formation of multilayers on wood surfaces.
3. Compare the two techniques, dipping and spraying for assembly of polyelectrolytes to wood surfaces.
4. Determine mechanical performance of LbL-modified wood as a function of layer number using shear tests.

CHAPTER 2 – LITERATURE REVIEW

2.1 Layer-by-Layer (LbL) assembly

2.1.1 What's LbL

Layer-by-Layer self-assembly (LbL) is a nano-scale technology that is recently developed by scientists to yield films with nanoscale control over their architecture. LbL refers to the adsorption of oppositely charged polymers, polyelectrolytes, in sequential adsorption steps to yield a multilayer film with a defined layer sequence on a given substrate (Figure 2.1). The binding force that connects the adjacent layers is largely based on the electrostatic attraction between oppositely charged macromolecules. And in some cases, except for the Coulomb interaction described above, hydrogen bonds [1, 2], donor/acceptor interactions [3], adsorption/drying cycles [4, 5], covalent bonds [6,7], stereo complex formation [8] or specific recognition [9] can also contribute to the binding force substantially based on the type of polymers.

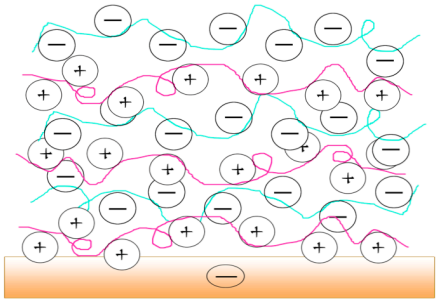

Fig 2.1 Schematic showing the simple formation of multilayers on given substrate.

LBL is open to a wide range of molecules as adsorbing reagents. These materials can be small organic molecules, inorganic compounds, macromolecules, biomacromolecules, colloidal scale metallic oxides or latex particles. Instead of combining molecules by chemical reactions in classic synthesis, in LbL deposition, molecules interact with each other by electrostatic attraction to enable the formation of a sequence of layers. The structure is a strict arrangement similar to atoms within a molecule. Also, the involved molecules will show their original properties, when there is no chemical reaction happens within the layers. So, the modification of surface can be kept in control [10].

In addition to having a wide spectrum of adsorbing reagents, LbL technique has

another advantage of requiring no specific shapes or materials for the substrates. It is only required that the material exhibits a non-zero surface charge. With regards to the morphology of substrates, LbL coating methods can be divided into two categories: coating on planar substrates and coatings on colloids. The fabrication of one single bi-layer of polyelectrolytes to a planar substrate can be generalized by four basic steps (given a negatively charged substrate): 1) the substrate is dipped into a polycation solution for 10~20 min; 2) the substrate is removed and dipped into to pure water to remove excess polymer; 3) the substrate is transferred into another solution that contains polyanions for 10~20 min; 4) the rinsing step is the same as described in step 2; 5) the process is then repeated from step 1 to 4 for additional bilayers fabrication, as Figure 2.2 shows. Similarly, the coating on colloids can be obtained by mixing the particles with polyanions and polycations dispersions with intermediate washing and centrifugation steps to remove excess polyions [11, 12].

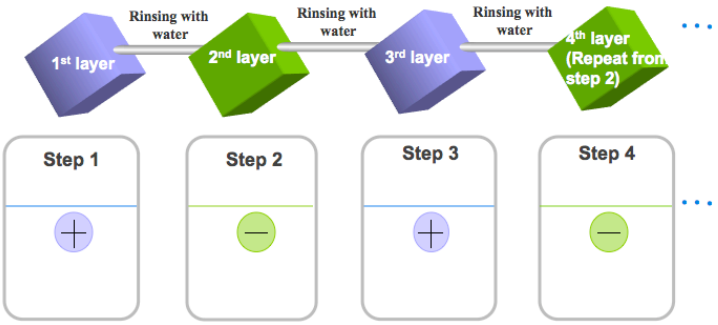

Fig 2.2 Schematics demonstrates the simple LBL procedure to fabricate multilayers on given substrates.

2.1.2 Three zones in polyelectrolytes multilayer films

Though LbL self-assembly is described as the build up of numbers of polyelectrolyte layers, the layers in the film actually do not have distinct separation. Layer interpenetration has been reported in the multilayers by many studies [10, 23, 29, 30]. Interdigitation between polyelectrolytes can occur within a multilayers film adsorbed to a substrate, and the film can be divided to three distinct regions with regards to the locations in a film (Figure 2.3). The first one is Zone I, which is comprised of one or a few polyelectrolytes layers close to the substrate. Layer interpenetration cannot happen in

this zone because of the repulsive force between the polyions and the surface charges. Zone III is the outer part of a multilayers film where one or a few polyelectrolyte layers are influenced by the solution or air. In this zone, the terminating polyions have a portion of their chains interacting with the previously adsorbed layers with loops and tails extended to the solution [10].

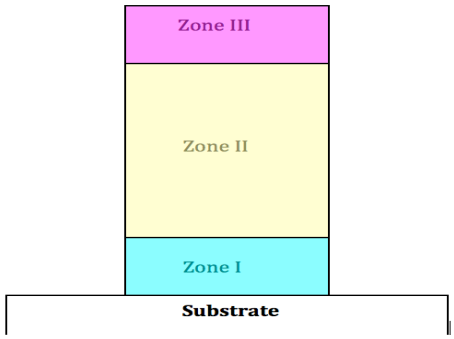

Fig 2.3 Diagram shows the three zones on a substrate.

Zone II is a “bulk” film, between Zone I and Zone III, which is not influenced by either interface. In Zone II, adjacent layers interdigitate with each other and ‘fuzzy layers’ are formed instead of stratification of each layer. This phenomenon has been studied by researchers [10, 29,30], and it was observed that for each polyion layer, one third of it segments was complexed with the underlying polyion layer, and one third on the other side interpenetrated with the polyion layer on its top. Schlenoff J. B [23] has given a kinetics approach to the adsorption of polyelectrolytes. He revealed that the deposition can be divided to two steps: the first step involves a rapid adsorption of charged polyelectrolytes to the surface with opposite charges, and the second step involves the rearrangements of the adsorbed polymer chains within the inner part of the previously deposited layer. The interdigitation of polyelectrolyte layers should happen during the second step. A schematic is given below (Figure 2.4) to show the zone model in a polyelectrolyte film. Also, it should be noted that the change from one zone to another one is gradual, so there is actually not a distinct boundary to distinguish which layer is the beginning of each zone.

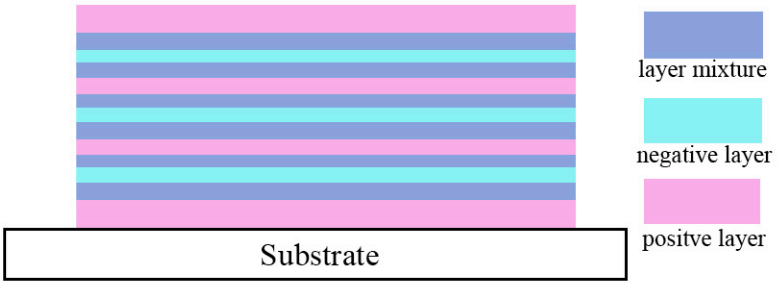

Fig 2.4. Diagram shows the interpenetration of polyelectrolyte layers in a multilayer film.

2.1.3 History of LBL

LbL assembly is a successful method for the formation of nanostructured films, the principle of which was firstly reported by Iler in 1966[13], and the conception of the work was first used by Hong and Decher [14]. In previous work when scientists were seeking a method to put amphiphilic molecules in one-dimensional order in a thin film, Langmuir-Blodgett (LB) technique was mainly used to control the fabrication of nanostructured films. In this technique monolayers were formed on a water-air interface and then transferred onto a solid support [15]. However, the LB technique required special equipments and had severe limitations with respect to substrate size and morphology. Self-assembly techniques, based mainly on silane-SiO_2 and metal phosphonate chemistry, were developed in the early 1980s, as an alternative to LB films. Some disadvantages still existed, such as being restricted to certain classes of organics, and not be able to form a reliable high-quality thin films [15].

Therefore, the need for a simple way to fabricate a reliable multilayer film was filled by LbL self-assembly technique. Decher and co-workers began to study LbL technique in the early 1990s [14] led to the creation of multicomposite films composed of rod like molecules equipped with ionic groups at each end [16] or polyelectrolytes [14], and subsequently biobased microfibrillated cellulose [61] through LbL adsorption from aqueous solution. Their success in LbL technique realized the control of molecular orientation and organization on the nanoscale. Encouraged by the achievement on this novel technique, researchers from other fields such as chemistry, physics, material science, biology and medical science, etc. started to apply this technique to progress the field in utilizing LbL self-assembly deposition for nanoscale surface tailoring and

fabrication of nanoscale films [62-65].

2.1.4 Influence of salt content and pH on the formation of films

When polyelectrolytes are used for LbL, electrostatic attraction is the main driving force for film formation and the local ionic environment will influence the formation of multilayers. Especially when weak polyelectrolytes (polyelectrolytes with isoelectric points) are used, secondary forces such as hydrophilic/hydrophobic interaction and hydrogen bonding, etc. can also be a factor. It has been found that the molecular organization, composition, surface properties and chemistry of the multilayer film can be manipulated with suitable adjustments of the pH or ionic strength of the dipping solutions [26]. Salt, which can control the ionic strength of a solution, is known to participate in many aspects of LbL formations and functions, when added to the polyelectrolyte solutions. The incorporation of salt ions within a LbL film can be expressed by a equilibrium between "intrinsically" charge compensated polyelectrolyte complex, $Pol^{-}Pol^{+}$, where internal charge is balanced by polymer segments only, and an "extrinsically" compensated form, $Pol^{+}Cl^{-}$ and $Pol^{-}Na^{+}$, where salt counter ions participate in charge neutralization [27].

$$Pol^{-}Pol^{+} + Na^{+} + Cl^{-} \Leftrightarrow Pol^{+}Cl^{-} + Pol^{-}Na^{+}$$

Many studies report that polyelectrolyte multilayers can be formed with thicker layers in the presence of salt than the ones without [17-20]. Explanation given to this phenomenon is that the electrostatic charges on polyelectrolytes are screened by salts, thus the effective repulsion force on a polymer between segments or between polymers due to the same charges on the chains are reduced. Being less repulsed by adjacent polyion segments, polymers when adsorbed to the surface will trend have a coiled conformation instead of extended, and form flexible layers, as showed in Figure 2.5.

Fig 2.5 Schematics demonstrates the structure of polyelectrolyte layers adsorbed on given substrates under different salt conditions.

Though salt is capable of controlling the film thickness, it has also been determined that it can weaken the attractions between polyelectrolytes and substrates by screening the charges on polyelectrolyte chains to cause desorption of polyelectrolytes, as described in Kovacevic et al.'s work [8]. Further more, salt can affect the permeability of polyelectrolytes layers [21,22]. Harris and Bruening reported that high permeability of PAH/PAA multilayers could be obtained in the presence of salt [21]. Andreas and Fery reported that discrete nanopores in the multilayer films are accessible simply by immersing multilayers film prepared from salt-containing solution in pure water [22].

In addition to controlling the ionic strength, adjusting pH of the solution is another method to manipulate the organization and thickness of multilayers. Sensitivity of weak polyelectrolytes to pH conditions lead to their different degrees of ionization or different linear charge densities with varying pH. Weak polycations are fully protonated when pH is below its pK_a and becomes almost neutral when pK_a is approached. Shiratori and Rubner have used PAA and PAH, both of which are weak polyelectrolytes, to investigate the pH dependence of film thickness. In their studies when both polyelectrolytes were fully charged, very thin layers (<10 $\overset{o}{A}$) were obtained, and thickness increments were detected when one of the polyelectrolytes was barely charged. Also, if adsorbed multilayers are treated at pH conditions different from the one during adsorption, the multilayers will go through a rearrangement and even delamination may occur.

2.1.5 Comparison of dipping and spraying methods for LbL

LbL is normally preceded by cycling substrates to oppositely charged polymer solutions, as mentioned above, with rinsing step in pure water in between. However, this is not the only method for the LbL technique. In recent studies, there are publications showing that multilayers were deposited by sequential spraying of oppositely charged polymers to yield films of equivalent quality, composition, and morphology to those prepared by dip coating of substrate [23-25]. One advantage of adopting spraying in LbL is to decrease the time for approaching the maximum adsorption of one layer dramatically from normally 10~20min to only 6s. Also, given the same short adsorption time, multilayer films that were formed by spraying were proven to have higher quality

than the ones formed by conventional dipping methods [23]. Excess polyelectrolytes sprayed at the surface of a vertically oriented substrate are removed by drainage during spraying, in which case, the rinsing step can be skipped and, thus, speed up the buildup process [24].

2.2 Coating on wood

2.2.1 Application of wood coating

As a renewable natural resource on the earth, wood has been widely used in almost every aspect of our life with its comparable mechanical strength, texture, friendly aroma, and low density, etc. However, during the long history of human beings' utilization of wood, it is found that wood has disadvantage that it is susceptible to degradation when in contact with moisture, high temperature, chemicals and fungi etc. To eliminate the exposure of wood to severe conditions, coatings are applied to wood in industry to enable wood products to become more durable in the exterior environment. Various coating types have been introduced, such as the application of varnish, lacquer or paint for retardation of the change of moisture content, the utilization of fire-retardant for the improvement of fire performance, treatment of preservatives such as Chromated Copper Arsenate (CCA) for the prevention from fungi or rot, lamination of other materials such as plastics for decoration or isolation from moisture and sunlight, and coating of bonding agents for adhesion. In the wood composite area, where adhesives are commonly used to bond pieces of wood together, surface properties are highly related to the performance of adhesives. Chemical treatment of wood surfaces may enhance the bonding with a high degree. Especially for the adhesives that do not have good affinity with wood chemically, coupling agents are applied on wood to enhance the bonding between adhesives and wood, such as in Vick et al.'s work, hydroxymethylated resorcinol (HMR), which has been used for the bonding of epoxy to spruce [86].

2.2.2 Factors affecting chemical coating

Many issues influence the application and retention of coating applied to wood. Chemically, the components of cellulose, hemicelluloses, lignin and extractives in wood influence the retention and bonding between the coating chemicals and wood surface.

The various contents for each component, and the difference in extractives with regards to different wood species even make it harder to determine the chemical interaction between coating chemicals and wood. In this study, negative charges attributed to the dissociation of hydrogen from carboxyl groups and phenolics in wood are utilized for LbL assembly. The interaction of cationic polymers with anionic surface groups is expected.

In addition to the native chemistry, heterogeneous wood structure is another factor that play an important role in influencing the coating, especially in enabling penetration of chemicals into wood. Different cell structures in wood give (in this study, softwood is concerned) diverse degree of accesses to the chemicals, and influence of these units on the coating is discussed as below:

1. ***Tracheids*** : Elongated cell that composes around 90% volume of tissue. Average sizes of tracheids are 3.0 to 5.0 millimeters long and 30 to 45 micrometers width in diameter. When cut normal to the cell axis, many opening are available on the cross section of wood to enable polyelectrolytes access to subsurface layers of wood.
2. ***Rays without resin canals*** :(ray parenchyma cells, ray tracheids): These transversely oriented cells cover around 5~9% volume of tissue. The heights of ray vary in number of cells as viewed in tangential section. Normally, they range in number from six to nine per millimeter. When cut tangential to the cell stem axis, ray cell provide access to the interior layer of wood.
3. ***Pits*** : Pits are small opening present in the longitudinal tracheids that provide communication between tracheids or tracheids and rays. They can be divided into three categories: 1) intertracheal, which is between adjacent longitudinal tracheids; 2) pit pairs that are between longitudinal tracheids and ray parenchyma; 3) pit pairs that are between longitudinal tracheids and ray tracheids. The intertracheal bordered pits on the radial walls of early wood are numerous and their sizes are associated to the diameter of longitudinal tracheids. Normally there are one or two rows of pits across the width of the tracheid. These interlumen connections provide access from cell to cell. Access is limited by pit membrane type, with regards to border pits, and the torus may also limit access so the opportunity for polyelectrolytes to penetrate into wood.

4. ***Normal resin canals*** : normal resin canals distribute in both longitudinal and transverse directions of in wood, composing about 1% volume of tissue. The longitudinal canals in *Pinus* have an average of 200 micrometers in diameter and transverse canals are around 100 micrometers. Compared with tracheids and rays the diameter of resin canals is more greater. They may provide more access into wood since it is intercellular space with no connecting membrances.

2.3 Microscopes used to characterize polyelectrolytes adsorbed on wood

2.3.1 Confocal Laser Scanning Microscopy (CLSM)

Confocal laser scanning microscopy (CLSM) is an advance optical microcopy built on conventional fluorescence microscopy. CLSM has superior imaging ability to light microscopy because of its ability to produce single plane images. With a laser illumination source and adjustable detectors for detecting fluorescence of different wavelengths, CLSM enables simultaneous, multi-band fluorescent imaging [37]. In the CLSM, as showed in the Figure 2.6, a laser beam is used to illuminate a small spot at the focal plane of the fluorescence labeled specimen. When a mixture of illuminated fluorescent light from the specimen and reflected laser light is traced back to a detector, a beam splitter will allow only the laser light to pass into the detection apparatus. After passing through a pinhole, which blocks the fluorescent light not from the focal plane, the focused fluorescent light reaches the detector and is recorded by a connected computer. An image from the specimen is built up by scanning the spot in a square raster pattern. A computer controlled scanning mirror between objective and beam splitter helps to move the laser beam in X-Y direction to collect the whole fluorescence information at one focal plane, which lead to a two-dimension image. At the same time, if the beam scans stacks of planes at Z direction, a 3-dimension image will be obtained.

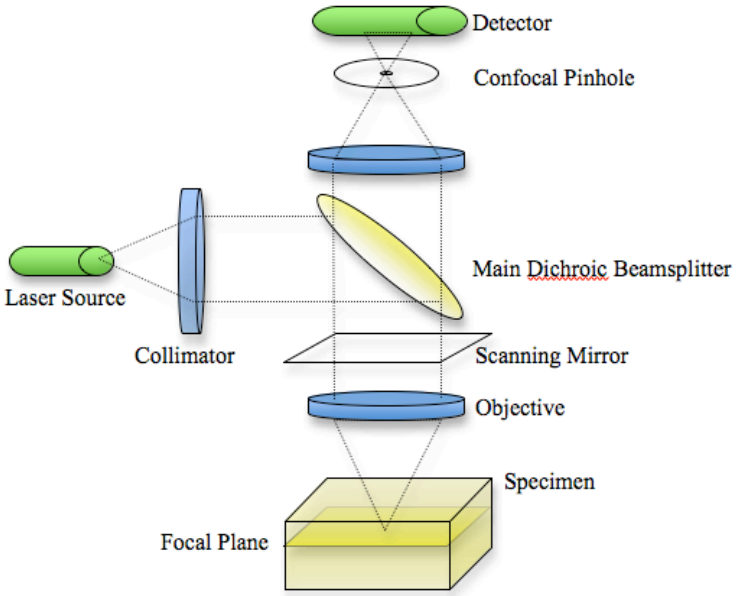

Fig 2.6. Schematic of CLSM.

In the field of wood science, CLSM had been used to get 3-dimensional images of xylem cells, to detect ortho-quinones in wood, to visualize liquid flow pathways in wood, to monitor wood microfracture, to analyze the lignin distribution across wood fiber and to draw the profile of bordered pit aspiration [31-36]. In contrast, scanning electron microscopy (SEM), which was widely used to characterize the microstructure of wood, has the disadvantage of requiring conductive coating, being operated at vacuum condition and requirement of zero percent of wood moisture content. CLSM however, needs no specimen coating and can work at ambient air pressure with normal relative humidity. [32] In the study of showing the profile of pit aspiration, a conventional fluorescence microscopy would require many sample sections to obtain enough information. However, confocal laser scanning microscopy, which allows observation of internal structures along the Z-axis in specimens, makes it possible to observe thick sections without embedding, and under a range of moisture conditions. [35]. Another example of CLSM is in wood bio-deterioration research, where labelled hyphae of *O. piceae,* could be contrasted against the strong autofluorescence of wood cell walls and extractives [37].

2.3.2 Environmental Scanning Electron Microscope (ESEM)

In contrast to the Scanning Electron Microscope (SEM), ESEM has the advantage of being able to operate at gaseous environment with low pressure, no requirement of conductive coating and without the need to dry the samples [38]. As seen in Figure 2.7, electrons generated from the gun hit the sample surface and induce emission of secondary electrons (SEs) from the sample. These SEs collide with the gas molecules to generate more SEs and are accelerated by the detector and an electron 'cascade' is formed, leaving the amplified signal. Around the electron gun, the pressure is kept at 10^{-6} to 10^{-7} torr, and at least 10 torr around the sample. Gas in the sample chamber can be nitrous oxide, carbon dioxide, helium, argon nitrogen and water vapor. Among them water vapor is most commonly used due to its relevance to biological samples [39]. If water vapor is in the sample chamber, hydrated samples can be used directly without further drying process.

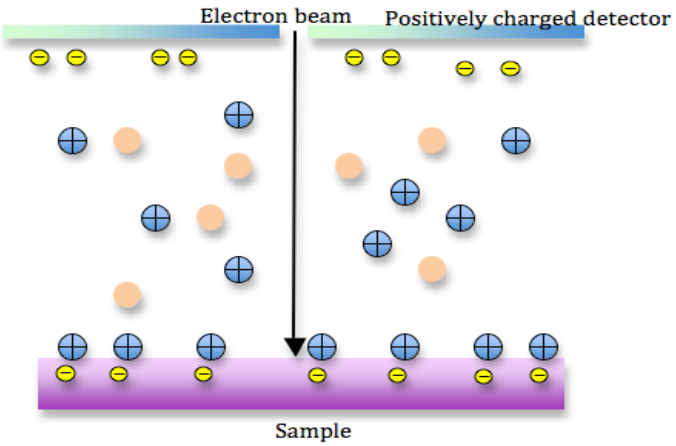

Fig 2.7 Schematic of ESEM.

In the area of wood science, ESEM has been used by many groups to examine the micrographic structure of wood or fiber surface. In the field of wood preservatives studies, Craciun et al. has used ESEM to observe the nano size copper dimethyldithiocarbamate crystal deposited on wood cell wall-lumen interface; both Fruhmann et al. and Sippola Merja et. al. have done *in situ* tension tests of pine inside the chamber of an ESEM to study the wood fracture surface on cellular level. In the former study examination of wood specimens with 12% moisture content was successfully achieved. In recent studies of fiber surface modification, ESEM was used to detect the nano scale coating of

polyelectrolytes on fibers, further more, even surface roughness can be obtained by applying image analysis to the ESEM images [28].

2.2.3 Fourier transform infrared spectroscopy (FTIR)

FTIR is an analysis technique that provides information about the chemical bonding or molecular structure of a specimen. FTIR analysis can be applied to minute quantities of materials, whether solid, liquid, or gaseous. The technique works on the fact that bonds and groups of bonds vibrate at characteristic frequencies matching wavelengths of infrared light. FTIR spectroscopy uses infrared light emitted by a light source and channel towards an interferometer. The interferometer consists of a fixed mirror, a moving mirror and a beamsplitter. IR from the source is divided into two optical beams by the beamsplitter. One beam is reflected off of a fixed mirror, another beam reflects off of a moving mirror that is away from the beamsplitter. These two reflected IR beams will recombine when they meet back at the beamsplitter and an interferogram resulting from the interference of the two beams is obtained. The interferogram signal exits the interferometer and is focused upon the sample, any molecule that meets the radiation will absorb the infrared energy at a specific frequency. The radiation intensity passing through the sample is measured by the detector, and a FTIR spectrum containing the information of molecular absorption and transmission information is created. By interpreting the absorption peaks in a FTIR spectrum, molecules or molecular group in the specimen can be identified. FTIR spectrometers should be purged by dry CO_2 free air, since both H_2O and CO_2 can absorb infrared radiation. A simple layout of spectrometer is shown in Fig 2.8.

FTIR has been widely used in the field of LbL assembly technique, and to determine the interaction of components in the multilayer film is one of its applications [40-44]. In this study, FTIR is utilized to exam the cross linking between PAA and PAH, which are the main components in the multilayer films. Previous research indicated that the amine groups of PAH and carboxylate groups of PAA cross-linked and formed amide bonds at temperature between 130°C~160°C and this conversion could be detected by FTIR [42-44].

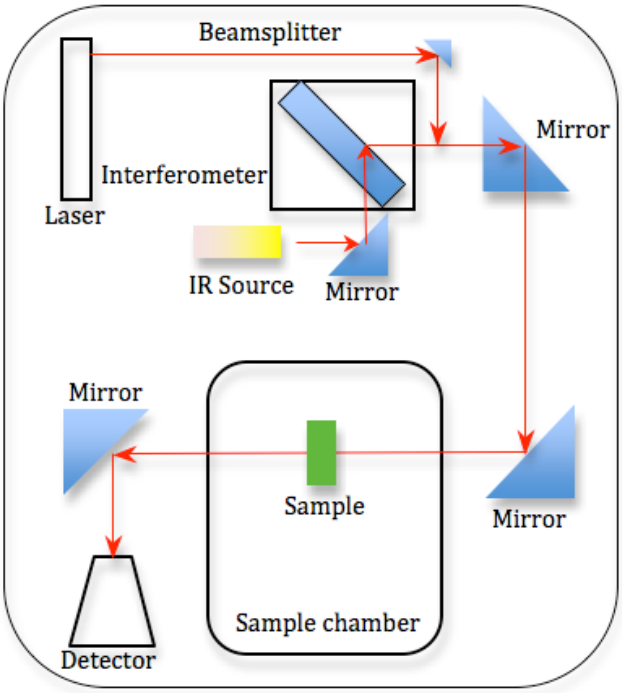

Fig 2.8 Simple layout of a spectrometer.

2.4 Zeta Potential measurement

Zeta potential measurement is conducted based on the electric charges that most microscale particles obtain in aqueous colloidal dispersions. Particles are generally charged for three reasons: the ionization of its surface chemical groups, the differential loss of ions, and the adsorption of charged species. When a particle is charged, its counter ions will tend to gather around its surrounding area and form an electric double layer, within which there is an inner (stern) layer composing of the ions that are strongly bonded to the particle and an outer (diffuse) layer formed by the loosely associated ions. Within the diffuse layer, the balance of electrostatic force and random thermal motion determines ion distribution, and in this region a boundary (slipping plane) exists, within which the particle together with its closely bonded ions act as a single entity. When this particle is placed in an electric field, the potential at the boundary is called zeta potential ζ (Figure 2.9). This zeta potential is closely related to the type and amount of charges the particle have, so it is a function of the surface charge of a particle and ionic strength of the solution.

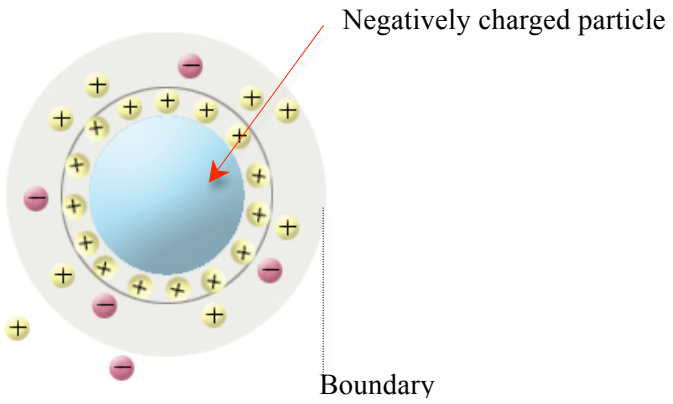

Fig 2.9. Schematic of a charged particle with its associated double layer.

Zeta potential can be determined by measuring the mobility, which is also the velocity of a particle when it is placed in an electric field. In the electric filed, particles are induced to move back and forth by altering the charge between the electrodes. At the same time, the movement of particles is monitored by scattered light obtaining the velocities of particles, as shown in Figure 2.10. Zeta potential can be calculated by Smoluchowski's formula as shown below:

$$\zeta = \frac{4\pi\eta}{\varepsilon} \times U \times 300 \times 300 \times 1000$$

where ζ is zeta potential (mV); η is the viscosity of solution; ε is the dielectric constant; U is the electrophoretic mobility and equal to v/(V/L), v is the speed of particles (cm/sec); V is voltage (V) and L is the distance of electrodes.

Zeta potential measurement has been widely used to study the stability of colloids and flocculation processes. In recent LBL study, zeta potential measurement is mainly used to detect the reverse of surface charges on the particle when oppositely charged polyelectrolytes are adsorbed to the particle surface. [46-48]

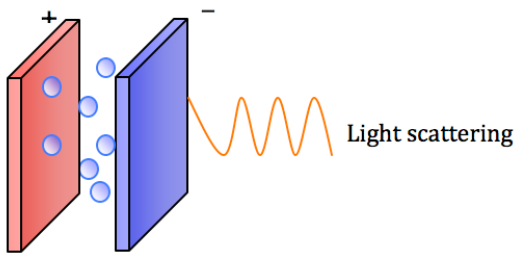

Fig 2.10 Schematic of charged particles in an electric field.

2.5 Carbon-Nitrogen-Sulfur Analyzer

The Vario MAX CNS analyzer (Elementar, Hanau, Germany) is used to determine carbon, nitrogen, and sulfur contents in food, plants and soil by weight of each element (note: this result may vary given different measured sample sizes). In this technique, a sample is carried by a reusable crucible and burned in an excess of oxygen at up to 1200°C, and the gas analysis process is outlined below:

Combustion:

$$R\text{-}N+O_2 \rightarrow N_2+ NO_x+O_2+CO+CO_2+CH_4+X^-+SO_x+H_2O$$

Post combustion:

$$CO+CH_4 \xrightarrow{CuO\&Pt} CO_2+H_2O$$

Reduction:

$$NO_x+O_2+SO_2 \xrightarrow{tungsten} N_2+WO_3+CO \text{ (trace)}$$

$$CO+CuO \rightarrow CO_2$$

After the combustion, carbon content is obtained by the adsorption of CO_2 in purge and trap column, nitrogen content is measured by the detection of N_2 using a thermal conductivity detector. After analysis the remaining ash is collected on a storage tray. This technique has been widely used in the agricultural research such as soil analysis [49-51], examination of food [52] and plant tissue studies [53,54], etc. A range of sample sizes is suitable for CNS analyzer, while specific sample amount may be desired with regard to the different kinds of materials, such as, when plant tissue samples are measured, weights of about 300 mg per measurement are generally sufficient for CNS quantification. Also, if the desired nitrogen or carbon contents are too high or too low, less or more than 300 mg of this sample should be used because of the sensitivity of the detector has a measurement range (0.02 to 30mg for N, 0.02 to 200mg for C and 0.02 to 15mg for S).

2.6 X-ray photoelectron spectroscopy (XPS)

XPS is a surface chemical analysis technique that utilizes photoelectric effect and energy-dispersive analysis of the emitted photoelectrons to characterize changes of the chemical composition of a material surface. In the XPS equipment, an X-ray beam of with the energy of $h\nu$ is emitted from the source and irradiates the sample surface. As the

X-ray photon is absorbed by an atom in a molecule on the sample, a core electron of the atom will get ionized and emit from the sample surface. The kinetic energy of the emitted electron (E_k) is then collected by an analyzer, and the XPS spectrum is obtained. The relationship between the photon energy ($h\nu$) and the electron kinetic energy (E_k) is shown as the equation, $E_k = h\nu - E_b$, where E_b is the binding energy (BE) of the electron, and it is a characteristic parameter that is associated with every specific core atomic orbital. Therefore, as the equation shows, since the given photo energy is fixed, the electron's kinetic energy can be utilized to characterize chemical components in a surface. XPS has been used in the area of wood science to characterize surface chemical modification for many applications, such as the examination of extracted red oak, black cherry and red pine surface [55], surface analysis of different wood species [56], identification of heating effect on wood chemical composition by studying the changes of O/C ratios [57], determination of wood surface condition after the treatment of hydroxymethylated resorcinol [58] and evaluation of surface lignin on cellulose fibers [59].

On the wood surface, the main signals are derived from carbon and oxygen, attributed to the abundance of carbohydrates contained in wood. With regards to the C 1s signal from wood, it is commonly divided into four states according to the number of oxygen atoms bonded to C:

C_1: carbon atoms that are bonded only with carbon or hydrogen atoms, and its binding energy (BE) is around 284.6 eV. It is found that this carbon component is mainly from lignin and wood extractives;

C_2: carbon atoms that are bonded with one non-carbonyl oxygen atom, which appears at a higher BE compared to C_1 ($\Delta BE = +1.5 \pm 0.2eV$), and it arises mainly from cellulose;

C_3: carbon atoms bonded to one carbonyl oxygen atom from lignin, hemicelluloses and extractives, or two non-carbonyl oxygen atoms from cellulose and hemicelluloses, with BE compared to C_1 ($\Delta BE = +2.8 \pm 0.2eV$);

C_4: carbon atoms bonded to one carbonyl and one non-carbonyl oxygen atom from hemicelluloses with BE compared to C_1 ($\Delta BE = +3.75 \pm 0.2eV$) [78].

2.7 ASTM-D905 Compression Shear Test

The ASTM-D905 shear test is used to determine the comparative shear strengths of adhesive bonds for wood or other materials. Since this test can be affected by the strength of wood, the loading condition, stress distribution in the samples and even adhesives used, etc., the obtained shear strength may not truly represent the shear properties of adhesives. Hence this test is primarily applied as an evaluation of adhesive for wood and similar materials. The standard D905 specimen is a single overlap joint that has a glued area of 18.75 cm^2 and is tested in compression, as shown in Figure 2.11 &2.12.

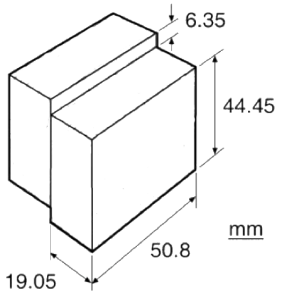

Fig 2.11 Geometry of the standard ASTM-D905 specimen.

During the test, compression load is constantly applied by two rigid surfaces until failure starts in the bondline or in the material (Figure 2.12). The shear strength is calculated by the equation: $\sigma = P_{max} / A$ (where σ is the shear strength (N/mm^2); P_{max} is the maximum load when failure starts; and A is the bond surface area (mm^2)). The breaking surface is also examined to determine the material failure, defined as the percentage of material contacting the adhesive that remains in the bondline after testing [60]. When wood are bonded together by very strong adhesive, wood failure is commonly seen and the measured shear strength may be lower than the actual adhesive shear strength.

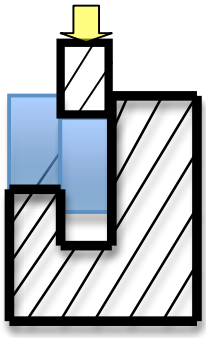

Fig 2.12 Shear compression test model in the United Testing System.

CHAPTER 3 – RESEARCH METHODOLOGY

3.1 Materials

A. Polyelectrolyte solutions.

Poly (acrylic acid) (PAA, MW=100,000), poly (diallyldimethylammonium chloride) (PDDA, MW=100,000~200,000), poly (allylamine hydrochloride) (PAH, MW= 70,000), poly (ethylenimine)(PEI, MW= 25,000) and poly (fluorescein isothiocyanate allylamine hydrochloride) (FTIC-PAH, Mw~15,000, $\lambda_{max} = 494nm$) were purchased from Sigma Aldrich. Fig.3.1 shows the repeat unit structure of molecular structures of the listed polyelectrolytes. All solution were prepared using ultra-pure deionized water (Milli-Q plus system, Millipore) with a resistivity of 18.2 MΩ•cm. Polyelectrolyte solution were freshly prepared by diluting concentrated polyelectrolyte solution with water in a beaker and stirring for 2 hours.

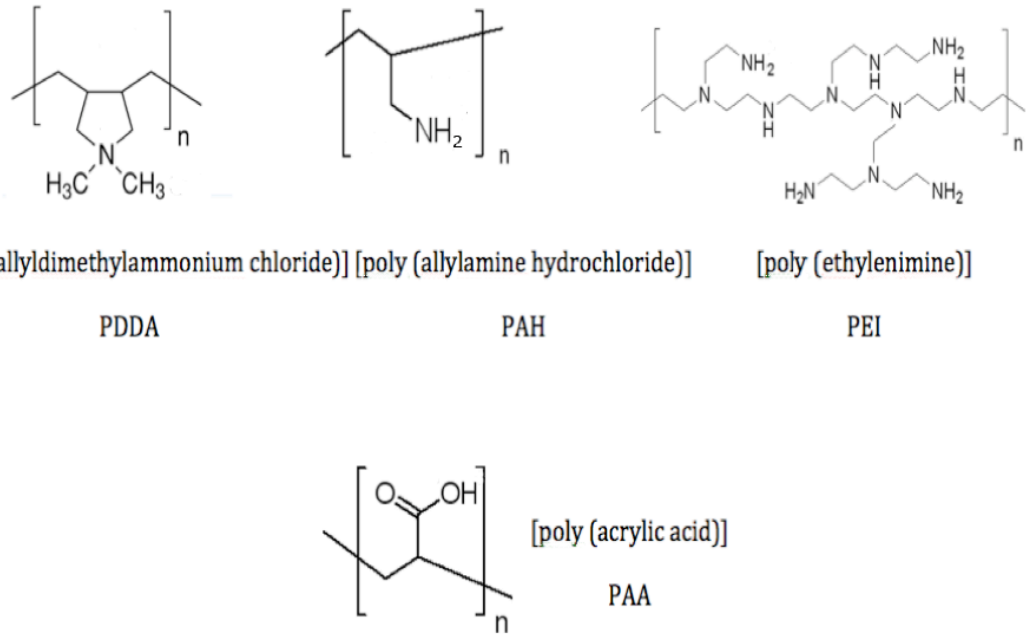

Fig.3.1 Schematic representation of molecular structures of polyelectrolytes used for LbL assembled films (shown without counterions for clarity).

B. Wood

Specimens of different geometries were cut from a group of gymnosperms *Pinus spp.* classified as southern yellow pine and saturated with water before all treatments (details of the wood soaking method were included in the Method section) (Figure3.2). All the wood samples came from sapwood. For XPS analysis (section 3.1.1.3), CNS measurement of the optimal adsorption of PEI (section 3.1.1.5), early wood was predominately used.

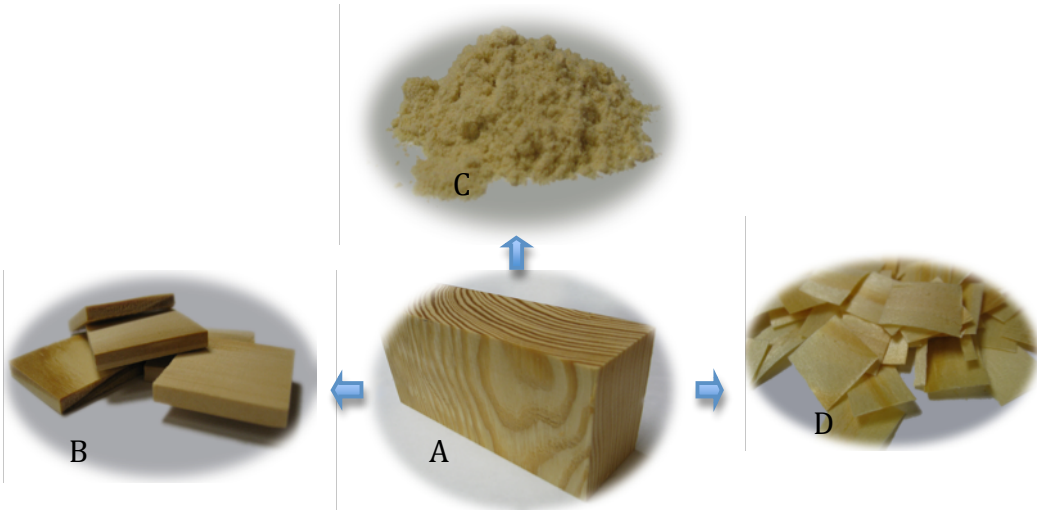

Fig 3.2. Geometries of wood specimens used in this project. A) Wood block from which all specimens were cut; B) wood blocks where thin sections are cut for fluorescence microscopy and CLSM observation; C) wood powder used in zeta potential measurements; D) wood flakes used for XPS analysis, CNS measurements, ESEM examination and spraying experiments.

3.2 Method

3.2.1 Evaluation of influence of pH and ionic strength on polyelectrolyte adsorption to water-saturated wood

3.2.1.1 Surface potential of wood under different pH

Wood samples were ground into fine powder using a Wiley Mill (model.4) passed through 140-mesh screen. A series of wood powder suspensions were then prepared by adding 1mg wood powder to 100mL Milli-Q water that had been adjusted to a pH of 3, 5, 7, 9, 11 and 13 with HCl and NaOH. After Waiting 10 min for the sedimentation of large particles, the supernatant solution containing fine particles was separated from the sediments. The pH of all suspensions was measured again and recorded. The supernatant was then placed in a disposable capillary cell (DTS1060) for zeta potential measurement, which was conducted by a Zetasizer Nano ZS (Malvern Instrument Ltd., Worcestershire, UK). For each sample, six measurements were taken.

3.2.1.2 Surface potential of wood after the adsorption of PDDA and PEI under varying pH

To apply the first cationic layer of polyelectrolyte on wood, 1mg of wood powder was added to 100mL PDDA or PEI solutions, which had been prepared to a concentration of 10mg/mL and adjusted to a series pH of 3, 7 and 10.5 with HCl and NaOH. The deposition time was 30 min with stirring at room temperature. After one layer was applied, solutions were set aside for 10 min until large wood particles settled out of suspension, and the supernatant solution with fine particles was isolated from the sediments. All samples were washed twice with ultrapure Milli-Q water by centrifuging at a speed of 4900rpm for 10min. The washed particles were again added to Milli-Q water to make 100mL suspensions. Before zeta potential measurements, the suspensions were slightly shaken by hand. After waiting 10 min for the sedimentation of large particles, the supernatants of solutions containing fine particles were placed in disposable capillary cells (DTS1060) for Zeta potential measurements. For each sample, six measurements were taken.

3.2.1.3 Detection of PDDA and PEI by X-ray photoelectron spectroscopy (XPS)

A: Preliminary tests for one layer of PEI or PDDA coated samples.

10mg/mL PEI and PDDA solutions were freshly prepared with varying pH and salt content following the parameters listed in Table 3.1. Wood wafers with dimensions of 0.75cm by 0.9cm by 0.15cm were cut from early wood and saturated with water. To fabricate a film of a single layer of polyelectrolyte, wood samples were added to 100mL of polyelectrolyte solution. After 20 min of stirring using a magnetic stir plate, the flakes were transferred into Milli-Q water for another 15min. of stirring. Finally, the wood flakes were transferred to a vacuum oven (29mmHg) to dry at 40°C for 48 hours. Two replicates were included for each condition.

The XPS analysis was performed on a Perkin Elmer 5400 X-ray photoelectron spectrometer with a magnesium anode (X-ray-voltage 13kV, 250W, X-ray energy 1253.6eV). Samples were mounted on a stainless steel sample holder with tape. Before analysis, the wood samples were kept in a test chamber connected to liquid nitrogen to prevent the release of moisture from the wood until the pressure in the analysis chamber is not higher than 1.5×10^{-7} Pa. All spectra were recorded at a 90° angle on a surface area of approximately $1mm^2$ on the wood wafers. Survey spectra were recorded in 1.0eV steps and 89.45eV analyzer pass energy, and the narrow scan with 0.1eV steps and 17.9eV pass energy.

Table 3.1 Experimental parameters to apply one layer of PEI or PDDA

Condition	Polymer	Polyelectrolytes conc. (mg/mL)	pH	Salt conc. (mol/L)	Dipping Time (min)	Rinsing Time (min)
1	*PDDA	10	7	0	20	10
2	*PDDA	10	7	0.25	20	10
3	*PDDA	10	11	0	20	10
4	*PDDA	10	11	0.25	20	10
5	*PEI	10	7	0	20	10
6	*PEI	10	7	0.25	20	10
7	*PEI	10	11	0	20	10
8	*PEI	10	11	0.25	20	10
9	PEI	4	7	0	20	15
10	PEI	4	7	0.25	20	15
11	PEI	4	10	0	20	15
12	PEI	4	10	0.25	20	15

*Both water-saturated and water-unsaturated wood flakes were used for each condition.

B: Evaluation coated PEI on wood by XPS

Samples were prepared in the same way as described in 3.1.1.3, while following different conditions as listed in Table 3.2. Two replicates were included in each condition, and three points of 1mm^2 were scanned for XPS analysis within two flakes. The XPS analysis was performed on a PHI Quantera SXM-03 Scanning Photoelectron Spectrometer Microprobe (XPS, also known as ESCA) with a monochromatic Al anode (X-ray energy 1486eV). Samples were mounted on a stainless steel sample holder with tape. Before analysis, the wood samples were kept in a test chamber until the pressure in the analysis chamber was vacuum pumped to less than 1.5×10^{-7}Pa. All spectra were recorded at a 45° take off angle on a surface area around 1mm^2 on the wood wafers. Survey spectra were recorded in 1.0eV steps and 280eV analyzer pass energy, and the narrow scans were recorded with 0.1eV steps and 26eV pass energy.

Table 3.2 List of the experimental parameters to apply one layer of PEI on wood

Condition	Polyelectrolytes conc. (mg/mL)	pH	Salt conc. (mol/L)	Dipping Time (min)	Rinsing Time (min)
1	10	3	0	30	15
2	10	7	0	30	15
3	10	10.5	0	30	15
4	10	3	0.1	30	15
5	10	7	0.1	30	15
6	10	10.5	0.1	30	15
7	10	3	0.5	30	15
8	10	7	0.5	30	15
9	10	10.5	0.5	30	15
10	10	3	1	30	15
11	10	7	1	30	15
12	10	10.5	1	30	15

3.2.1.4 Quantification of adsorbed PEI on wood under different pH and salt contents by Carbon-Nitrogen-Sulfur Analyzer (CNS)

Solution of 10mg/mL PEI were freshly prepared with varying pH and salt content following the parameters listed in Table 3.2. To minimize variability among the wood samples, 24 wood flakes (10cm by 7.5cm by 0.3cm) cut from one block were used. Each flake was cut into 12 equal-size pieces and each piece was assigned to one treatment respectively. Therefore, two wood flakes pieces would be included for each treatment. To

fabricate one layer of PEI on wood, the wood flakes were placed in 100mL PEI solution. After 30 min of stirring, the wood flakes were removed, placed in Milli-Q water and stirred for another 15 min. After coating with PEI, all the wood flakes were dried in a vacuum oven (29 mm Hg) at 40 °C for 48 hours. A comparison test aimed at studying the penetration of polyelectrolyte into wood was conducted by soaking wood blocks (2.5cm by 2.5cm by 0.3cm) in PEI solutions. All solutions were prepared the same as described above. To apply PEI to wood, three wood samples were soaked in 100mL of PEI solution for each condition for 24 hours. After treatment, all the samples were soaked in ultrapure Milli-Q water for another 24 hours. All treated samples were dried by the same method as mentioned above in this section.

To quantify the PEI adsorption on wood, all treated samples were analyzed by a Vario MAX CNS analyzer (Elementar, Hanau, Germany). Before CNS measurement, all the wood samples were ground into particles and kept dry in a conventional oven at 60°C. For each measurement, 300mg sample was weighed and put in a reusable crucible. Three measurements were carried out for each condition. After weighting, all crucibles were placed in an orderly manner in a dish of the CNS analyzer. During each measurement, one crucible was picked up by a robot arm and put into the CNS instrument for analysis.

3.2.1.5 PEI adsorption isotherm on wood

A series of PEI solutions were prepared with a series of concentrations as listed in the Table 3.3 and adjusted to pH 10.5. Wood wafers with dimension of 0.75cm by 0.9cm by 0.15cm were cut from early wood. For each PEI solution condition, 20 wafers were treated following the same layer-by-layer (LbL) procedure as described in section **1.4**. After LbL treatment, all samples were transferred to a vacuum oven (29mmHg) for drying at 40°C for 48 hours. Before analysis, all samples were kept dry in a conventional oven at 60°C.

Table 3.3 List of PEI concentration in solutions for adsorption isotherm.

Condition	1	2	3	4	5	6	7	8
PEI conc. (mol/mL)	0.05	0.1	0.5	1	3	5	8	10

PEI adsorption was analyzed by the Vario MAX CNS analyzer (Elementar, Hanau, Germany). For each condition, three measurements were carried out. CNS measurements were the same as mentioned in section 3.1.1.4, except that 5 wood wafers were weighed for each measurement instead of 300mg samples.

3.2.2 Quantification of multilayers deposition on wood

3.2.2.1 CNS measurement of wood coated with PEI $(PAA/PAH)_n$

Wood was prepared in the same way as described in section **1.4** to obtain the precursor layer of PEI. Negatively charged PAA and positively charged PAH were then alternately applied following conventional LbL assembly procedures to form multilayers [14]. Polyelectrolytes solutions were prepared so that the final polyelectrolyte concentrations were 3×10^{-2}M expressed in unit of monomers per volume unit (monomol= moles of the respective monomer repeat unit). Thus, PEI at 10mg/mL, PAA at 6mol/mL, and PAH at 2.7mol/L were prepared respectively. The PEI solution was adjusted to pH 10.5, while both the PAA and PAH solutions were adjusted to a pH of 5.

The PEI $(PAA/PAH)_n$ multilayer assembly procedure was as follows: 1) wood flakes were added to100mL PEI solution for 30 min adsorption time with stirring; 2) the PEI solution was replaced with Milli-Q water and stirred for 15min to rinse away any loosely bonded PEI; 3) the second anionic layer was applied by placing rinsed wood flakes in the PAA solution following the procedure as for PEI with a subsequent rinsing step; 4) treated wood was transferred to PAH for the third layer; 5) additional layers were fabricated by repeating step 3 and 4. With the LbL assembly procedure, wood flakes coated with PEI$(PAA/PAH)_n$ (n= 1,2,3,4,5) were prepared and dried in a vacuum oven (29 mm Hg) at 40°C for 48 hours. Before CNS measurement, all wood flakes were ground into particles and kept dry in a conventional oven at 60°C. In the CNS analysis, three measurements were carried out for each sample. For each measurement, 300mg sample was weighed, the procedures were the same as mentioned in section 3.1.1.4.

3.2.2.2 Observation of wood coated with PEI $(PAA/PAH)_n$ by Confocal Laser Scanning Microscopy (CLSM).

Wood blocks with dimensions of 3cm by 3cm by 0.3cm were treated according to section 2.1 with 1mg/mL FTIC-PAH. After the LbL assembly procedure, wood blocks were coated with PEI$(PAA/FTIC\text{-}PAH)_n$ (n= 1,3, 5). In the wet state, coated blocks were cut with sliding microtome into 40μm thick transverse sections, as shown below, and mounted on glass slides for observation.

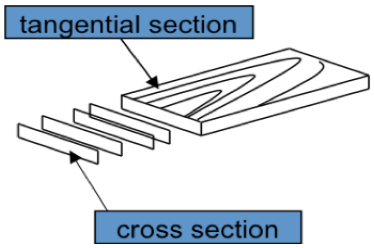

Fig 3.3. Schematic representation of cut away to obtain the transverse section.

Confocal microscopy experiments were performed on the a Zeiss LSM 510 Laser Scanning Microscope using an Argon and Enterprise (UV) laser as the excitation source. He sections were observed using a C-Apochromat 40×/1.2 water immersion lens. Confocal images were acquired at 1024 by 1024 pixels displayed on two separate channels represented by green and blue wavelengths for each channel. Images from these two channels were combined as an overlay imaged and displayed in color. Excitation wavelengths of 364nm and 488nm were used for illumination. Images were captured at wavelengths through a band pass filter (385~470nm) and at wavelengths through a long pass filter (505nm).

3.2.2.3 Observation of wood coated with PEI $(PAA/PAH)_n$ by Environmental Scanning Electron Microscope (ESEM)

Wood flakes with dimensions of 1cm by1cm by 0.15cm were treated according to section 2.1. After the LbL assembly procedure, wood flakes coated with PEI$(PAA/PAH)_n$ (n= 1,5,9) were prepared with two replicates for each condition. Before ESEM observation, a 10nm thick Au/Pd layer was sputter coated on the specimen with a Cressington sputter coater. ESEM (FEI Quanta 600 FEG) was used to examine the treated

and untreated wood under a vacuum pressure of 0.82torr. Images with 100, 2K and 10K magnification for each sample were obtained respectively.

3.2.3 Substituted spraying for conventional dipping methods

3.2.3.1 Single layer of polyelectrolyte on wood by spraying

To carry out spraying for LBL on wood, Nalgene aerosol spray bottles purchased from Fisher Scientific Co. were used (ref. made of HDPE, PP cap and rubber gasket, 180mL in volume). Each bottle was filled with either solution or water and pressurized by repeatedly pumping the piston assembly in an up and down motion, 7-10 strokes, before use. The spray rate was determined to be 0.6mL/s.

To apply the first layer of FTIC-PAH to wood samples, 1mg/mL FTIC-PAH solution was freshly prepared and sprayed onto the tangential section of wood blocks (figure 3.4) that had the dimensions of 5cm by 5cm by 0.3cm. Following previous work [24], spraying time was 3s with 27s drainage time. Milli-Q water was then sprayed for 20s with 10s to remove non-adhering material. In the wet state, treated blocks were cut into 40μm-thick transverse sections, as shown in Fig 3.3, and mounted on glass slides.

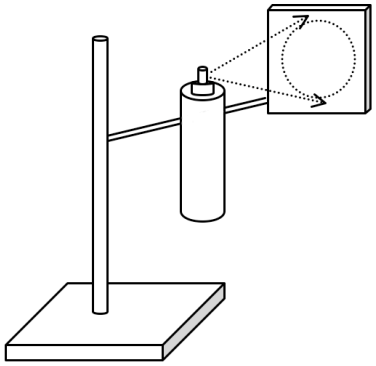

Fig 3.4 Schematic representation of spraying method for LBL self-assembly.

3.2.3.2 LbL assembled polyelectrolytes on wood by spraying.

Multilayers composed of PEI(PAA/PAH)$_n$ (n= 1,2,3,4,5) were applied to wood by spraying oppositely charged polyelectrolytes in cycles. Polyelectrolyte solutions were

prepared in the same way as indicated in section **2.1**.Two pieces of wood flakes in the dimensions of 10cm by 7.5cm by 0.15cm were used for each coating condition. The procedure for one layer coating as described in section 3.1 was used to apply multilayers to wood, the samples were sprayed with PEI, PAA, and PAH sequentially along with a rinsing cycle between each layer. After coating, all the flakes were moved to the vacuum oven (29mmHg) for drying at 40°C for 48 hours. All the wood flakes were ground into powder and kept dry in a conventional oven at 60°C before CNS measurements. In the CNS analysis, three measurements were carried out for each condition. In one measurement, 300mg sample was weighed and the procedures were the same as described in section 3.1.1.4.

3.2.4. Detection of cross-linking between PAH and PAA within a multilayers film on the model substrate

3.2.4.1 Coating on silicon surfaces

Silicon wafers were treated in a freshly prepared piranha solution (a mixture of H_2SO_4 (98%) and H_2O_2 (30%) with volume ration of 3:1) for 1h, rinsed thoroughly with water, and dried with a nitrogen stream. Solution of 0.6mg/mL PAA and 0.27mg/mL PAH were freshly prepared, and the pH of these solutions was adjusted to 5 with NaOH. Construction of the multilayer films was carried out by an automatic dipping robot, which was computer controlled. During the LBL procedure, silicon substrates were dipped into PAH and PAA solutions alternately with water rinsing in between steps in two separate bins. The dipping time in the polyelectrolyte and water rinse solutions was 15 and 5min, respectively. After the desired number of layers had been fabricated, the silicon wafers were dried with the nitrogen stream. Afterwards, each treated silicon wafer was placed in a glass vial and heated in the oven at a range of temperatures, which were 150°C, 170°C, 190°C, 210°C and 250°C for 2 hours, for each respective temperature. Before analysis, all the samples were stored in the test chamber to let its flowing dry air keep them dry. FTIR analysis was then conducted by a Thermo Nicolet 8700 Fourier transform infrared spectroscopy with 128 times scanning and a resolution of 8 cm^{-1} in transmission mode (note, silicon does not absorb IR light).

3.2.5. Mechanical tests

3.2.5.1 ASTM D905 test for strength properties of LBL bonding in shear by compression loading

Southern yellow pine was cut into 20 strips with the size of 32cm by 6.5cm by 2cm. with grain direction parallel to the longest dimension and soaked in water for a week. These samples were then used to form shear block specimens that contained layers of PEI(PAA/PAH)$_n$, a mixture of PAA and PAH, or phenol formaldehyde adhesive. After coating of each bonding material, the strips were kept to dry in a conditioning chamber with a relative humidity of 50±2% and a temperature of 23±1°C for a period of 7 days.

Coating:

The coating of multilayers with PEI, PAA and PAH follows the basic LBL procedure. Except for PEI solution, which was adjusted to a pH of 10.5 at 10mg/mL, each of the two other solutions was set to pH of 5 with a concentration of 8mg/mL. For each coating type, four wood strips were used. Among these four strips, two of them were coated with multilayers terminated with negatively charged PAA and two of them with positively charged PAH. Before application of PF, all four strips were soaked in an alkali solution of pH 10.5 for 30 min, and then in Milli-Q water for another 30min. After drying in the chamber as mentioned above, the PF with a solids content approximately equal to the total amount of PEI(PAA/PAH)$_9$ coating was spread on the tangential section of each wood strip. To apply the coating of mixture of PAA and PAH, the desired amount of each polyelectrolyte was measured in correspondence to its estimated adsorption amount in a multifilm of PEI(PAA/PAH)$_9$. The measured polyelectrolytes were then dissolved in a small amount of water and mixed together. The sediment was then separated from the water and spread onto the wood surface.

Hot press:

For each coating type**,** two coated wood strips were assembled and placed on the hot press, which had been preheated to 180°C. For the LbL coated wood specimens, strips coated with PAA and PAH as the respective terminal layers were assembled together after wetting the substrate. To wet the surface, water was sprayed horizontally to the vertically

placed samples by a spray bottle used in section 3.2.3 until the whole surface is wet. During hot pressing, two sets of assembled strips were placed in the hot press for 30min, with two pressure stages of 300psi and 150psi. The lower pressure was used during the first stage to soften the wood specimens and bring them into contact. After this, the higher pressure was applied to make complete contact between the two strips. Therefore, for the first 10min of pressing, the pressure of 150psi was applied and held; for the following 10min, the higher pressure of 300psi was applied and held; and for the last 10min, the pressure of 300psi was kept constant. After hot pressing, bonded specimens were kept in the conditioning chamber again for another 7days and cut into shear blocks as shown in figure 3.5. 28 shear blocks were obtained from each bonded strip.

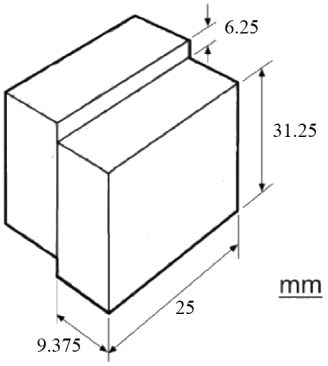

Fig 3.5 Geometry of the modified ASTM-D905 specimen.

Testing:

14 out of 28 shear blocks for each joint type were randomly chosen for mechanical testing in their dry state. All specimens were tested in a United Testing System apparatus and subjected to a compression load following the ASTM-D 905 standard. The loading speed of the machine during the experiment was set to 0.20in. /min. The load at the moment of failure occurs was recorded by the acquisition system and calculated into the shear strength.

The other 14 shear blocks for each joint type were then prepared for a weathering test. First, all specimens were boiled in water for 4 hours. After drying for 20 hours in a conditioning chamber, they were boiled again for a period of 4 hours and cooled in water. The same shear tests described above were then carried out on the wet samples.

CHAPTER 4 – RESULTS AND DISCUSSIONS

4.1 The effect of pH and salt content on polycation adsorption onto wood

4.1.1 Zeta potential measurements of wood as a function of pH

Zeta potential values of all wood samples were founded to be negative (Fig 4.1), and the values increased in magnitude when pH in the solution increased. As zeta potential values are related to surface charges of particles, the results indicate that wood surfaces are negatively charged and this anionic nature is enhanced at higher pH. Also, from Fig.4.1 it is observed that wood surface charge increase is not linear. A sharp rise exists when pH increases from 2 to 6, after which the rate of increase decreases as the zeta potential values approaches -30mV at pH>10.

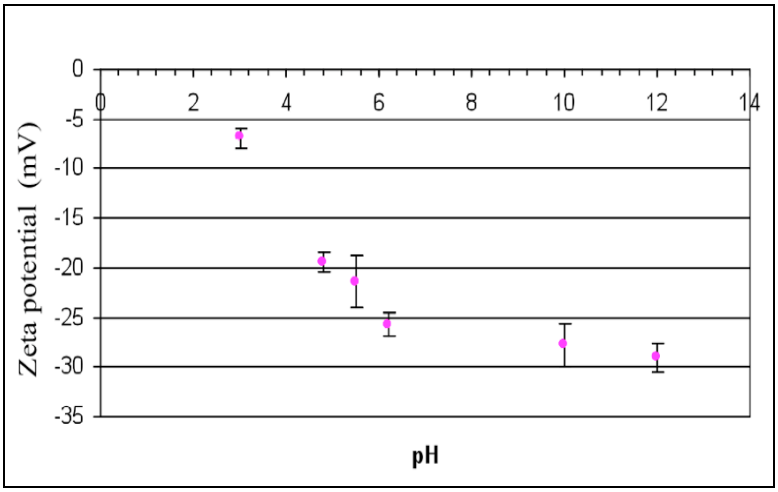

Fig 4.1 Zeta potential of wood particles as a function of pH. Average values were taken from 6 measurements. Error bars represent ±1 standard deviation.

At pH 4~6, the negative surface charge on wood may be attributed to the dissociation of hydrogen ions from carboxylic acids, including glucuronic acid on glucoronoxylan and galactoronic acid on pectin. When pH approaches 10, the aromatic biopolymer lignin, which has phenolic groups would start to deprotonate [75] and contributes to the slight increase in magnitude of zeta potential measurement.

4.1.2 Zeta potential of wood after the adsorption of PDDA and PEI under different pH

Adsorption of PDDA and PEI polyelectrolytes on wood as a function of pH was investigated by zeta potential measurement. PDDA is a polyelectrolyte that is permanently charged under any pH [80], while PEI is a weak polyelectrolyte that has varied degrees of ionization dependant upon pH condition. The negative zeta potential values reported for wood particles reversed to be positive after they were treated with cationic polyelectrolytes (Figure 4.2). The magnitude of surface potential increases as a function of pH of the treating solution (note: all measurements are performed with washed wood particles in Milli-Q water). Between PDDA and PEI, higher zeta potential values were obtained for PDDA than PEI under same conditions.

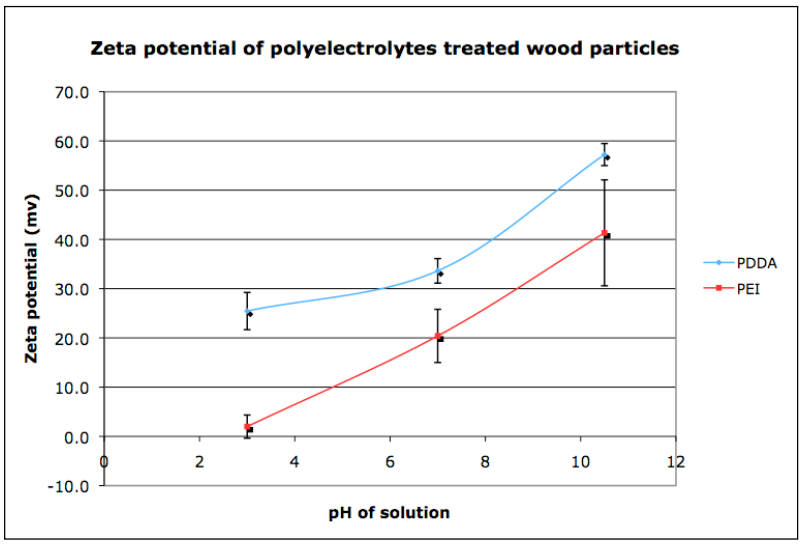

Fig 4.2 Zeta potential of wood particles that had been treated with PDDA and PEI at different pH. Average values were taken from 6 measurements in Milli-Q water. Error bars represent ±1 standard deviation.

There are two factors that can cause the increase of positive zeta potential on wood particles. One is the amount of surface charge on wood, and the other is the degree of ionization of polyelectrolytes. Since pH causes no change of the ionization of PDDA, the higher zeta potential is related to the increased negative charge on wood surface under elevated pH. When a PDDA molecule chain deposits on the wood surface, the ammonium ions contribute to the neutralizing of the wood surface charge, and the excess

cationic groups (loops and tails) are exposed to the solution making the wood surface positively charged. At higher pH conditions, wood surface has more negative charges to be neutralized by PDDA, hence higher density of charged wood particles is compensated by greater PDDA adsorption.

With regards to PEI, however, the deposition is different. PEI is a weak polyelectrolyte that is sensitive to its local ionic environment and has an isoelectric point pK_o. In the present system, the pK_o value of the primary amine in PEI is around 9, for the secondary amine around 8, and for the tertiary amine around 6-7 [26]. So, when pH of the polyelectrolyte solution changes, both the wood surface charge and degree of ionization of PEI will influence the deposition of PEI on wood. Also, when PEI is weakly charged, secondary interaction between wood substrate and PEI may also play a role in enhancing the adsorption [81].

At the treating condition of pH 3, which is below the isoelectric points of PEI, wood is less charged and PEI is almost fully charged. In this case, small amount of highly charged PEI in an extended conformation deposits on to wood. Since the electrostatic repulsion among the same polyelectrolyte will prevent its further adsorption onto the substrates, limited adsorption of PEI compensates the surface charges on wood. During the rinsing step the pH of the Milli-Q ultrapure water is around 6.5, in which condition ionization of PEI is changed and limited adsorption and conformation of the adsorbing polymer resulted in the low zeta potential values, which are almost close to zero.

In the case of pH 7 treating condition, surface potential on wood increased by 20mV (Figure 4.1) and as a result has potential to accept more positively charged PEI. However, at this time PEI becomes less ionized, more PEI is needed to compensate the surface charge on wood. The lateral rinsing step should not markedly affect this adsorption amount, as there is minimal pH change in the solution. Hence, the final zeta potential values show around 20mv, indicating increased adsorption amount of PEI at the wood surface.

Along with the increase of surface charges on wood at pH 10.5, the capability of

wood surface to accept positive polyelectrolytes is increased. Due to the low degree of ionization of PEI as it passes its isoelectric point, large amount of PEI is needed to compensate the negative charge on wood. Because at this stage, the surface charge on PEI is very weak, the ionic attraction between PEI and wood is decreased. Secondary forces such as hydrogen bonding between PEI and wood surfaces, as mentioned in the section of literature review, may play an important role to accomplish the PEI adsorption. The decrease of pH during washing step enables parts of the former neutral sites on the PEI chains to become ionized and the repulsion forces among polyelectrolytes chains become stronger. The final zeta potential of wood particles shows the highest values around 40mv at pH 10.5.

4.1.3 Surface chemistry investigation of wood coated under different pH and salt contents by X-ray photoelectron spectroscopy (XPS)

Zeta potential measurements are not effective for adsorption studies due to salt additives, because wood particles settle down after the adsorption of polyelectrolytes with salt. In order to quantify the adsorption of PEI on wood under different pH and salt contents, XPS was utilized to calculate the nitrogen contents on the wood surface, which originally derived from polyelectrolytes because wood has an inherently low nitrogen content.

4.1.3.1 Preliminary for detecting the first layer of PEI or PDDA on wood by XPS

The detection of coating of polyelectrolyte on wood was determined by the observation of nitrogen signal (wood itself is short of nitrogen, as shown in Figure 4.3) within XPS spectrum. It is observed in the XPS survey scan spectra that no nitrogen signal is detected from PDDA coated wood samples, no matter the treatment condition (Figure 4.4), while a small peak derived from nitrogen can be seen from the samples that have been treated by PEI (Figure 5). Signal related to chlorine Cl 2p3 can also be clearly seen due to the addition of salt.

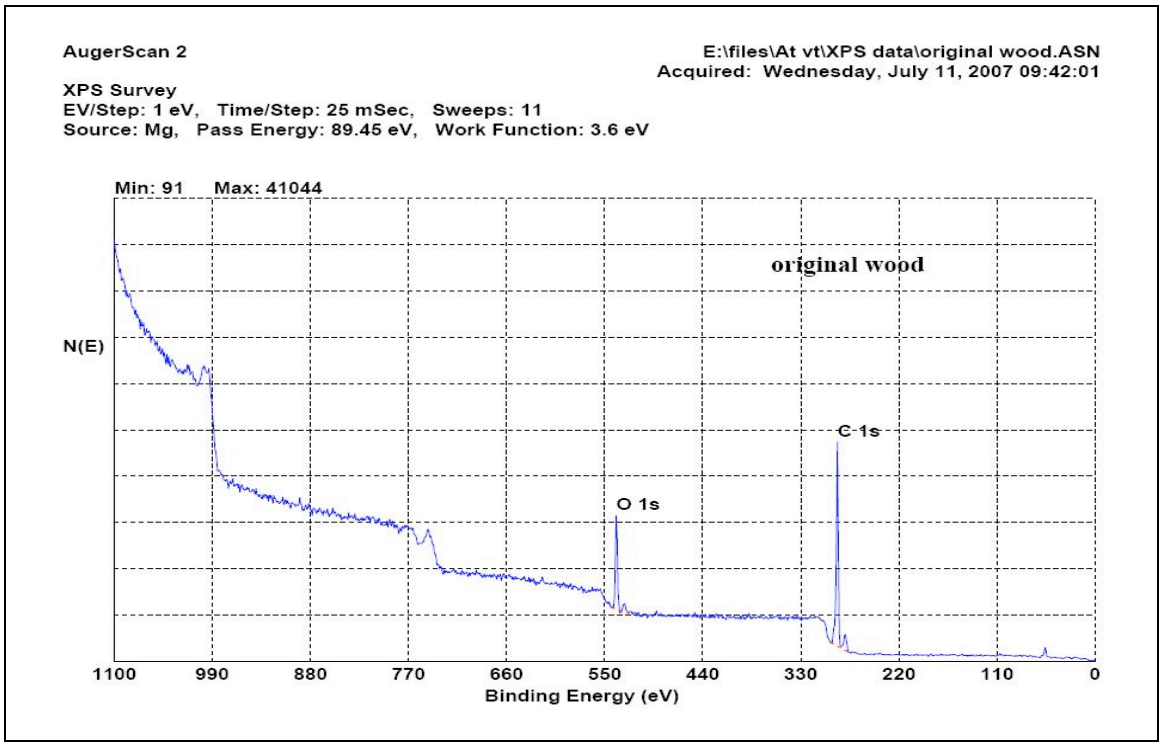

Fig 4.3 C 1s and O 1s XPS survey scan of original wood.

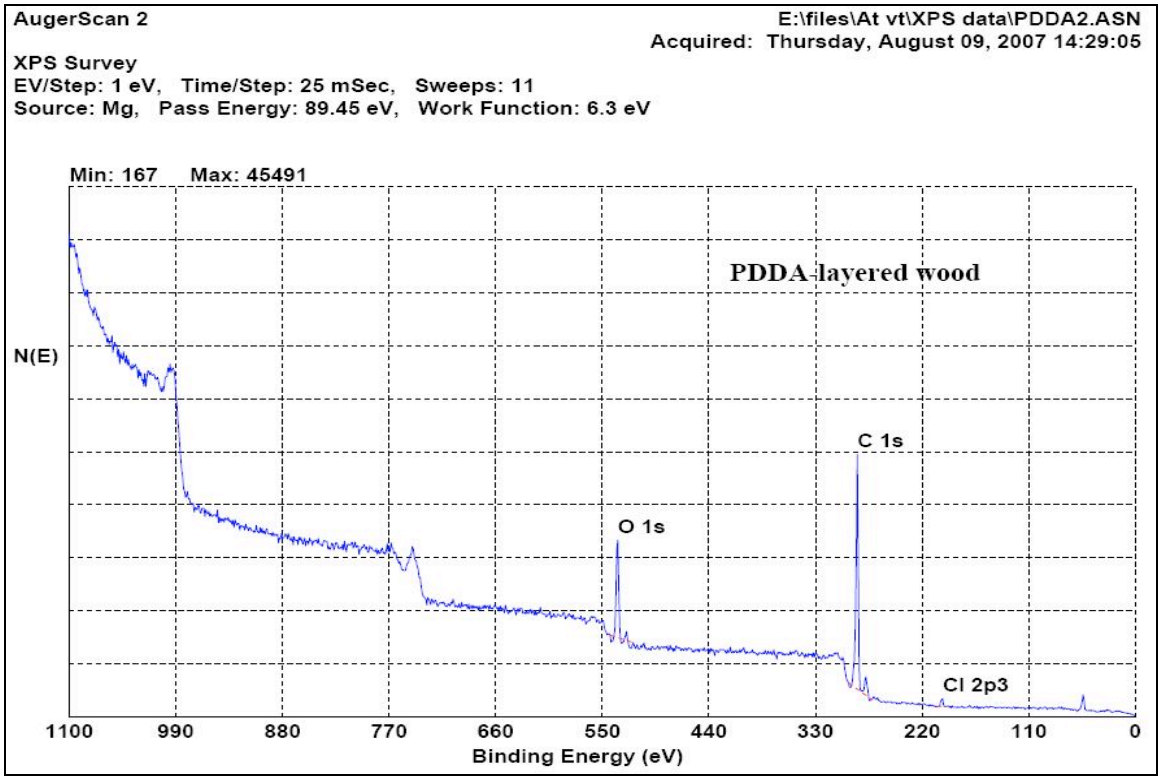

Fig 4.4 C 1s and O 1s XPS survey scan of PDDA-treated wood.

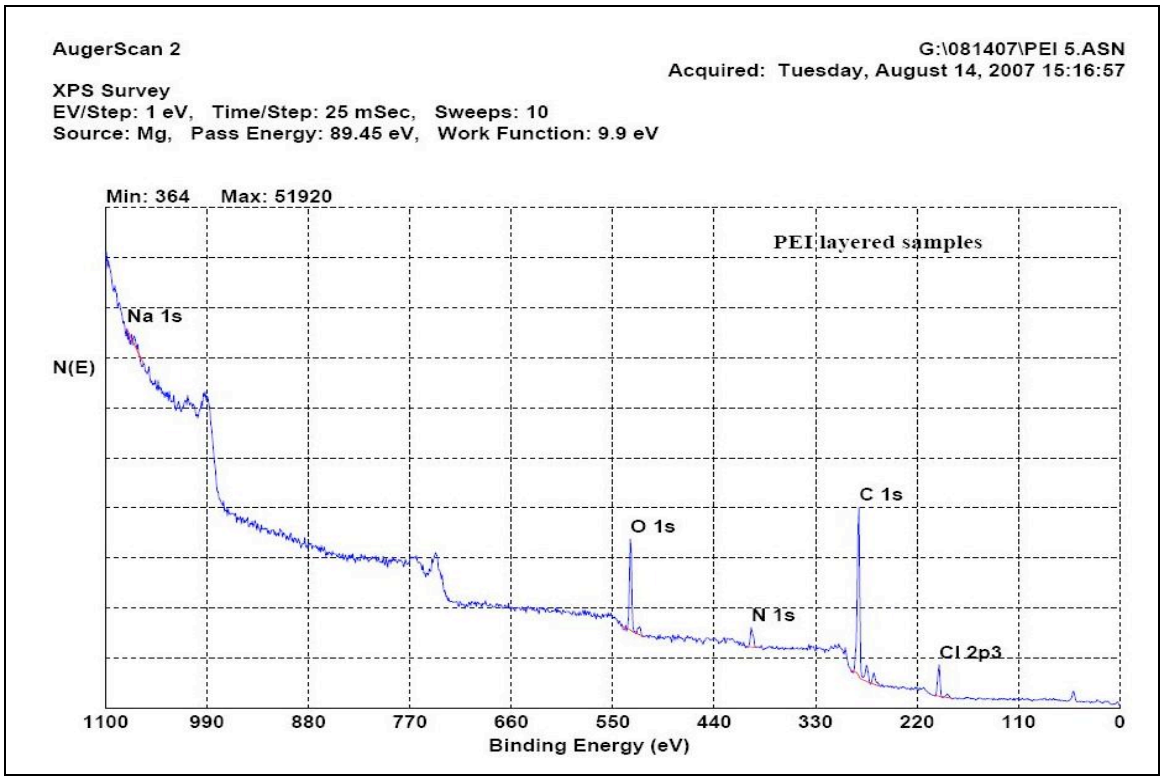

Fig 4.5 C 1s, O 1s and N 1s XPS survey scan of PEI-treated wood.

4.1.3.2 Quantification of PEI coating on wood by XPS

In figure.4.6, an XPS narrow scan of C1s peak of original wood with different carbon components are shown. The binding energies of 285.09eV, 286.84eV and 289.08eV can be traced to C_1, C_2 and C_3 respectively, and the relative proportion of each carbon was calculated to be 76.3%, 18.3% and 5.3% respectively. It has been established that C_1 mainly arises from lignin and extractives in wood and C_2 from cellulose [78]. The strong signal from C_1 in the spectrum suggests that high content of lignin or extractives are present on the wood surface. Similar carbon peaks are obtained from PEI coated wood samples, as shown in figure.4.7, however, the ratio of C_1/C_2 has changed significantly, with an increase of C_2 content to 31.1% and decrease of C_1 to 62.8%. The varying of C_1 and C_2 contents may be attributed to 1) the removal of lignin and extractives during the layer-by-layer process; 2) the presence of nitrogen and carbon linkage in PEI.

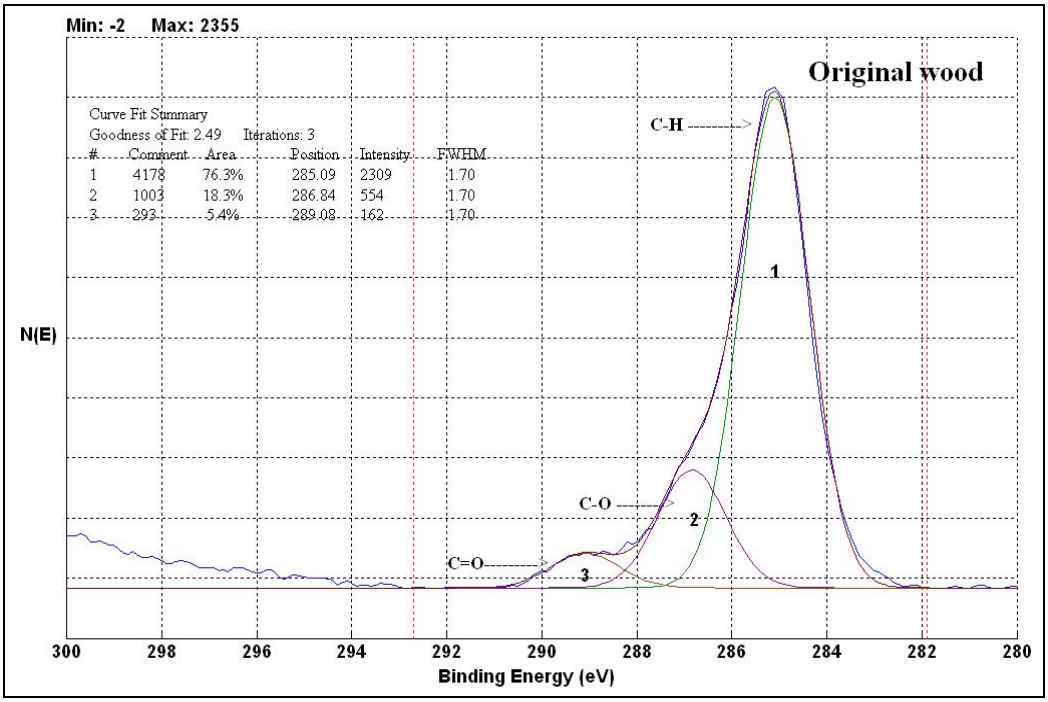

Fig 4.6 C 1s peaks of original wood.

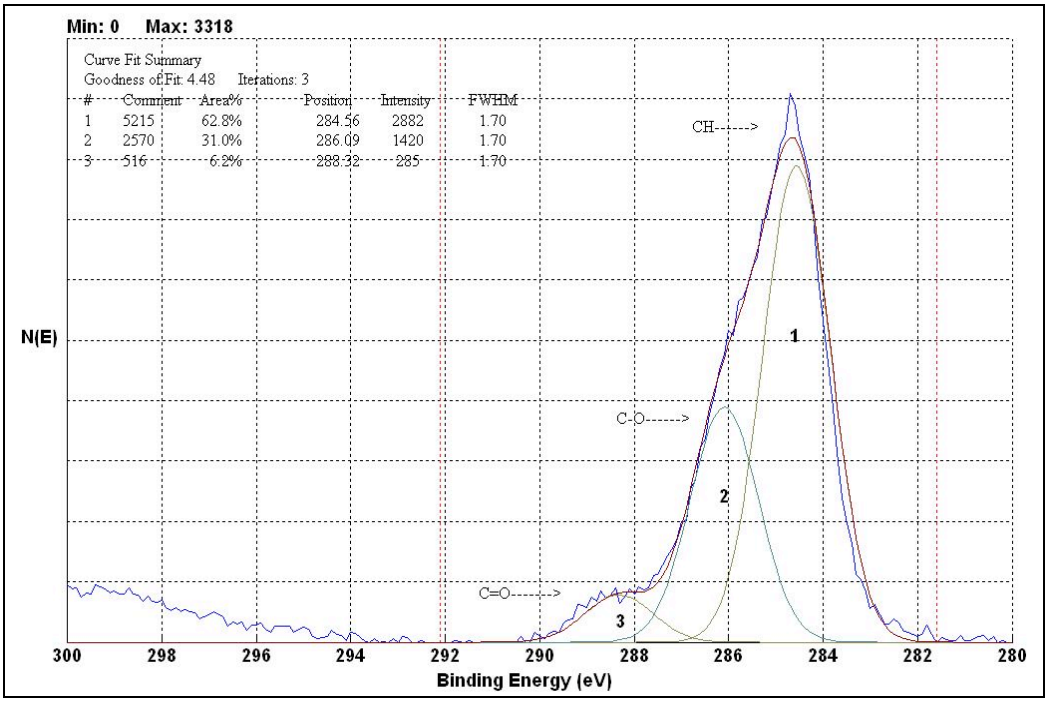

Fig 4.7 C 1s peaks of PEI coated wood.

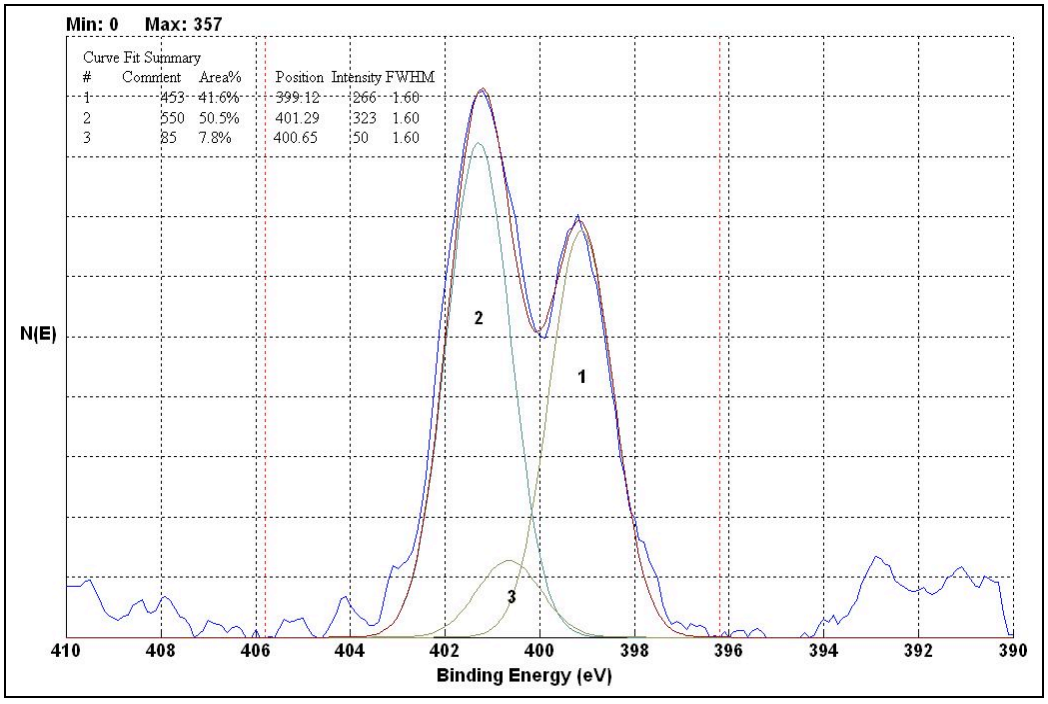

Fig 4.8 N 1s peaks of PEI coated wood.

Previous studies have shown that nitrogen from ammonium and amino groups have binding energies (BE) of 401.4eV and 399.3eV respectively [79]. Nitrogen peaks from PEI-coated wood are shown in figure4.8, clearly showing the N peaks from ammonium and amino groups at the BE of 401.29eV and 399.12eV, with relative areas of 50.5% and 41.6% respectively. Another possible nitrogen peak N_3 may be attributed to the urethane linkage between the nitrogen atoms and carboxyl groups in wood, but conditions for this reaction to occur is speculative at this point [79].

Comparisons of nitrogen contents in the samples that have been treated by PEI in different pH and salt conditions were carried out to determine the optimal condition for PEI adsorption. The first measurement shows, given constant pH, that the nitrogen content in PEI coated wood samples decrease as a function of salt content when salt concentration is below 0.5M, and shows a slight increase when salt concentration reaches 1mol/L. This trend is more prominent when the pH is at 3 and 7 at pH 10.5 there is no significant difference among the results for all salt conditions (figure 4.9).

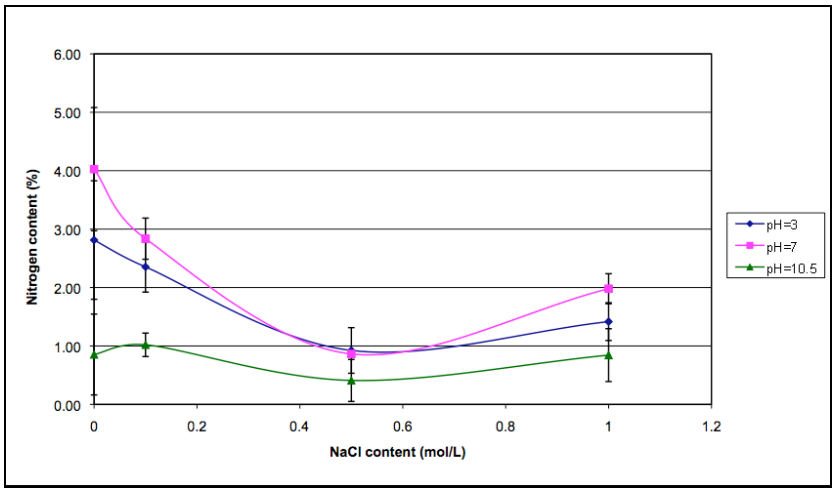

Fig 4.9 XPS results of nitrogen content on the wood samples that had been treated with PEI under different pH and salt contents. Average values were taken from 3 measurements. Error bars represent ±1 standard deviation.

XPS nitrogen analysis results were not reproducible, as shown in figure 4.10, when a separate experiment set was performed without the presence of salt. Lower nitrogen contents for pH 3 and 7, which is around 0.4%, were found than the former values, which were approximately 3.5%. No plausible explanation of why set's of samples varied. The variation is high among the results obtained from each treatment condition. Only when pH is at 10.5, similar results as the one from the first experiment are obtained. These values also have variation that prohibits determining the influence of pH and salt content on quantifying the adsorption of PEI to the surface of wood. Therefore the bulk nitrogen level of the different treatments is evaluated.

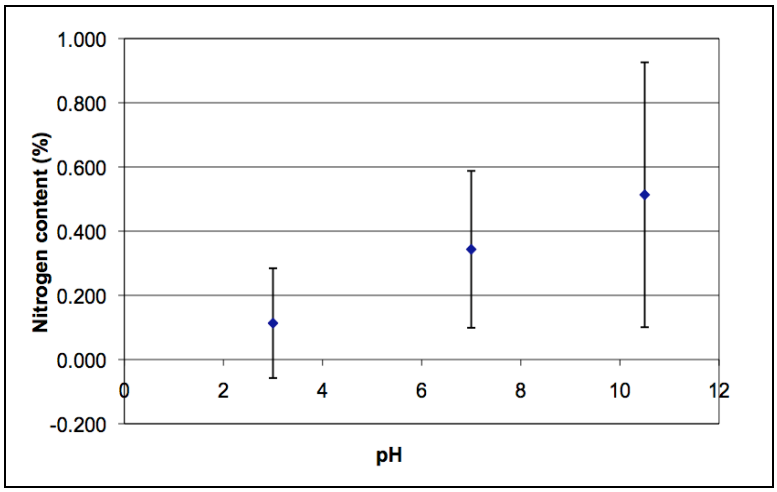

Fig 4.10 XPS results of nitrogen content on the wood samples that had been treated with PEI under different pH without salt. Average values were taken from 3 measurements. Error bars represent ±1 standard deviation.

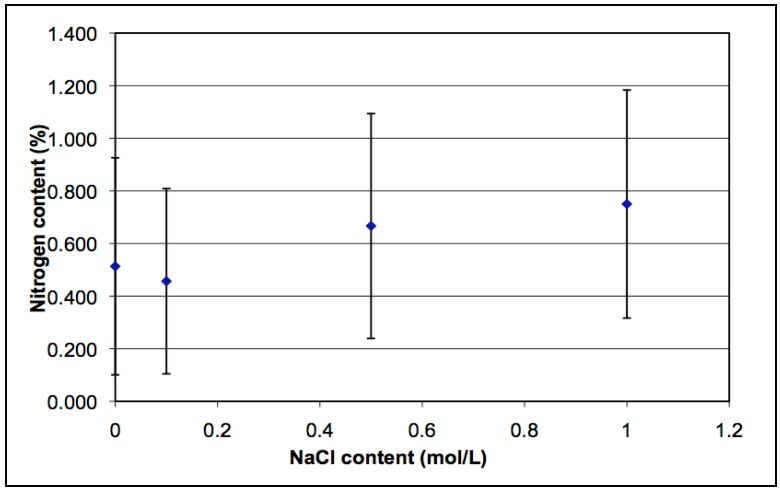

Fig 4.11 XPS results of nitrogen content on the wood samples that had been treated with PEI under pH 10.5 and different salt contents. Average values were taken from 3 measurements. Error bars represent ±1 standard deviation.

4.1.4 Quantification of first adsorbed PEI layer on wood under different pH and salt contents by Carbon-Nitrogen-Sulfur Analyzer (CNS)

Carbon-Nitrogen-Sulfur Analyzer (CNS) was used to quantify the adsorption of PEI on wood under different pH and salt conditions by incinerating the samples to measure the nitrogen content in PEI treated wood samples (Figure 4.12).

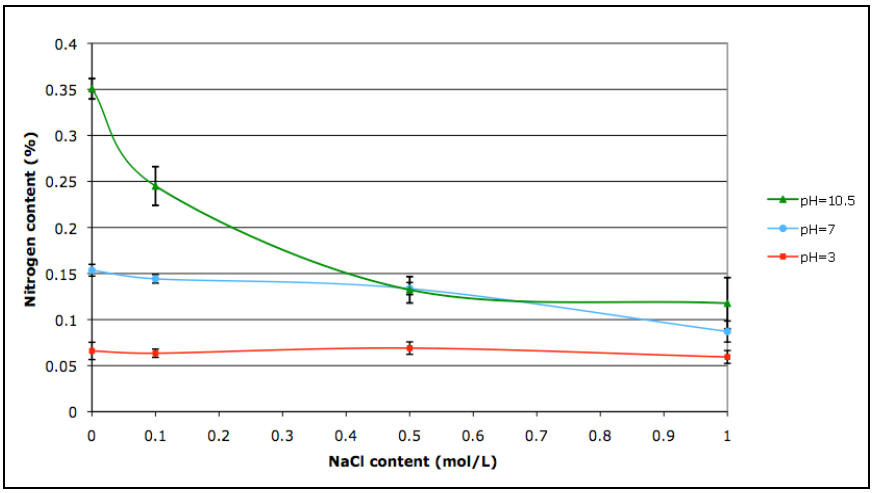

Fig 4.12 CNS data of wood that had been treated with PEI under different pH and salt contents followed by rinsing. Average values were taken from 3 measurements. Error bars represent ±1 standard deviation.

Wood is mostly composed of C, O and H with minimal N. Protein may contribute to the presence of nitrogen, but the total amount accounts for a small ratio of the mass of wood. As measured, the nitrogen content in southern yellow pine samples in this project was between 0.02~0.05%, while PEI was around 27% (measured by CNS). When PEI is applied to wood, the final nitrogen content on wood is greater than 0.05%, as seen in figure 4.12, and the amount of PEI deposited on wood at each condition can be quantified. By using the nitrogen content found in PEI, total mass ratio of PEI to wood was determined, as shown in figure 4.13 (see appendix for calculation).

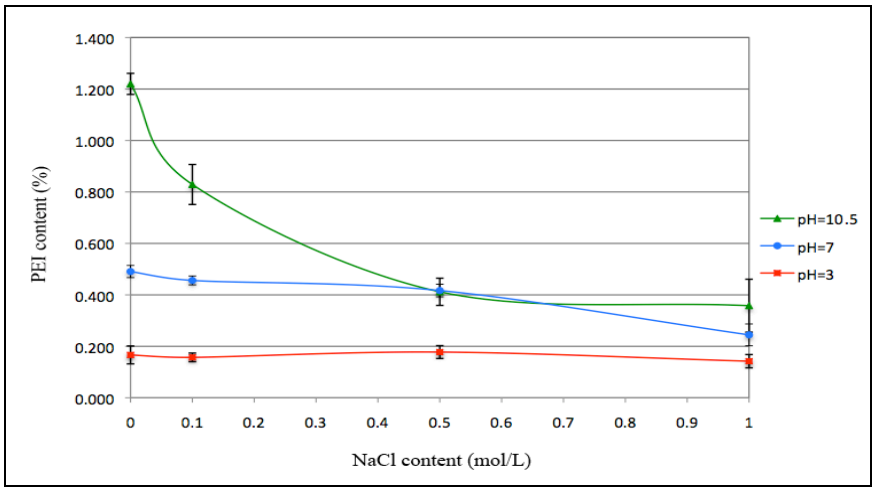

Fig 4.13 PEI adsorption calculated from the CNS data in figure.4.12. Average values were taken from 3 measurements. Error bars represent ±1 standard deviation.

At constant ionic strength, similar trends as the one from zeta potential measurements are found for treatment at different solution pH. Higher pH leads to higher adsorbed quantity of PEI. With increasing ionic strength at given pH, the results show varying trends for different conditions. At pH 10.5, there is a large decrease when salt is added, and adsorption is equivalent for pH 10.5 and pH 7 when the salt content increases to 0.5M. A decrease of PEI adsorption as a function of NaCl content at pH 7 is noted, but is not statistically significant. At pH 3, results from all salt condition appear to be consistently low and no decrease is observed in polymer adsorption as the ionic strength changes. The results show that salt has a negative influence on the adsorption of PEI to wood. One explanation is salt behaves as counterions in the solutions and competes with polyelectrolytes for the charged sites on wood. When more salt is added to the solution, these counterions occupy more charged sites on the surface and reduce potential PEI adsorption sites, as expressed in the equation below. Also, salt is capable of screening the charges on polyelectrolyte chains, which in other way effectively decreases the attraction between PEI and wood surface.

$$Na^{+}+Cl^{-}+Wood^{-}Pol^{+} \Leftrightarrow Wood^{-}Na^{+}+\ Pol^{+}+Cl^{-}$$

Similar explanation for reducing PEI adsorption by adding salt has also been reported

in Kovacevic et al.'s work [73]. In their study, they characterized the LBL multilayers as an ion-bonded glassy state at low ion concentration c_{ion}, 'liquid-like' at higher c_{ion}, and uncomplexed at very high c_{ion}. Salt ions can go into the dense phase to screen the attractions between polyelectrolytes, hence weaken the complexes [74].

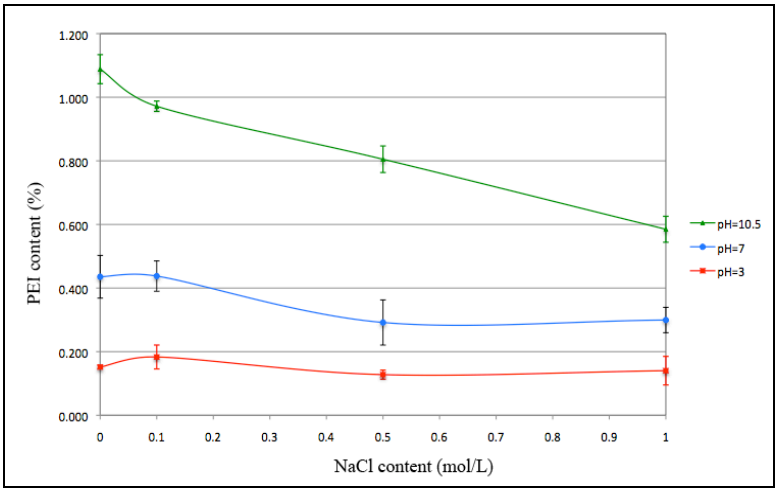

Fig 4.14 PEI contents in wood that had been soaked in PEI under different pH and salt contents for 24 hours and subsequently rinsed. Average values were taken from 3 measurements. Error bars represent ±1 standard deviation.

Wood is a porous material and CNS data are taken from a bulk system. Therefore the PEI contents obtained above may not actually represent its adsorption on the surface, but also include adsorption of PEI that has went into wood. To evaluate the location of PEI, a 24-hour soaking test instead of LbL half-hour dipping was performed. Results of nitrogen contents from CNS are converted to PEI content and shown as in Figure 4.14. After 24 hours soaking, without the presence of salt, for all pH environments, amounts of PEI adsorption are similar with the ones from 30 minutes treated wood samples (figure 4.13). Also, in the case of pH 3 and pH 7, no obvious difference is found. However, at pH 10.5 with addition of salt, PEI amounts are higher than the ones in LbL treatments, though they still decrease as a function of salt contents. It is suggested that the swelling of wood caused the increase of PEI adsorption at the higher pH and salt contents. In the alkali solutions, cell walls in wood are susceptible to swelling and more surface area is exposed. The presence of salt also enhances this swelling and enables more PEI adsorption at high

pH. However, the screening effect and counter ion adsorption reduce the attraction between PEI and wood so a decrease of PEI adsorption with increasing salt concentration is still observed.

4.1.5 Optimization of PEI adsorption on wood

In different LBL self-assembly studies, various polyelectrolyte concentrations in the dipping solutions have been used. Generally, in single study the same concentration was used for all the polyelectrolytes, and the most common used values are 0.5mg/mL [66], 1mg/mL [67], 2mg/mL [68-70], 3mg/mL [71] and 5mg/mL [72]. But in some research, a different method was approached for different polyelectrolytes, distinct concentrations are assigned, to achieve having the same moles of the respective monomer repeat unit for every polyelectrolytes [24]. To determine the optimal PEI concentration for its adsorption on wood, PEI solutions with a range of concentrations are applied to wood, and the resulting PEI contents are measured (Figure 4.15).

PEI adsorption increases with increased PEI concentration with a reduced rate of change. However, it is observed that even though PEI achieved the most adsorption of 0.67% content at its 10mg/mL concentration, after calculation (see appendix), only around 5.8608×10^{-3}g PEI exists on all wood samples. This amount of PEI can almost be provided by 100mL 0.05mg/mL PEI solution. Therefore, it is indicated that not all of the PEI in the solution contribute to the adsorption onto wood, and the PEI concentration should play an important role in controlling the maximum adsorption of PEI on wood. Bertrand et al. and Plech et al. [84, 85] have studied the kinetics of multilayer formation and suggest that polyelectrolytes adsorption involves a two-step process. In the first step, polyelectrolytes are transferred to the surface by diffusion so the electrostatic attraction can happen. The second step involves the self-arrangement of polyelectrolytes on the surface. In this case, the elevated PEI adsorption with high polyelectrolyte concentration should be explained by the diffusion in the first step. Higher concentration of PEI in the solution results in more PEI diffusing to the wood surface in the first place, until equilibrium is achieved between the PEI concentration in the solution and the ones surrounding the substrates. Additionally, as a polymer adsorbs, the system becomes more

ordered, losing entropy. Concentration of polyelectrolyte may have a role for this reason with regard to entropy of mixing.

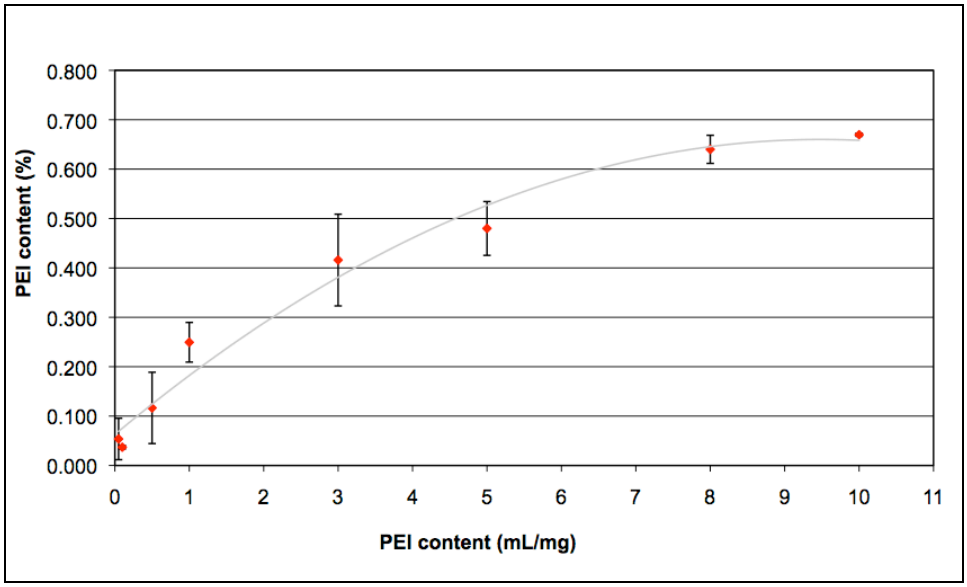

Fig 4.15 PEI content on treated wood samples as a function of PEI concentration in the solution. Average values were taken from 3 measurements. Error bars represent ±1 standard deviation.

4.2 Determination of multilayers film deposition on wood

4.2.1 CNS measurement of wood coated with PEI $(PAA/PAH)_n$

CNS measurements were performed to quantify the deposition of multilayers, PEI $(PAA/PAH)_n$ onto wood. Similar to PEI, PAH is also a polymer that has considerable nitrogen content (14.12% from CNS). Therefore, as multilayers containing PAH are continually fabricated on wood, increased nitrogen contents in the samples should be able to be detected. This nitrogen content can then correlate to PEI and PAH contents. CNS results in Figure 4.16 indicate that PAH contents of LbL treated wood increase as a function the number of LbL cycles (blue points in Figure 4.16), revealing the successful adsorption of each polyelectrolyte in every LBL dipping cycle. Linear growth of PAH contents is also found from the data with an increase in PAH content of 0.15~0.3% per layer. This is in contrast to the samples without PAA but repeated PAH dipping, where no increase of PAH mass is observed for all samples (red points in figure 4.16). There is even a slight decrease of PAH content after first adsorption.

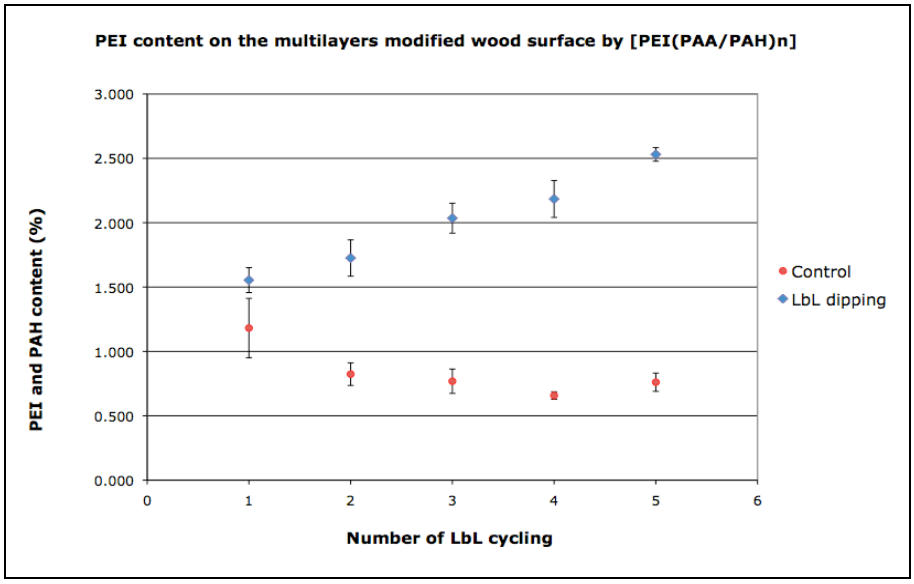

Fig 4.16 PEI and PAH mass contents (note: PEI was used only for the first cycle) on wood as a function of number of LbL cycles. Blue points demonstrate the samples prepared under normal LBL procedure; red points demonstrate the samples that were constantly dipped in PAH solutions. Average values were taken from 3 measurements. Error bars represent ±1 standard deviation.

This finding is consistent with the results of previous work where multilayers film fabricated by PAA and PAH is a typical example of the system. With this system there is a linear relationship between the mass or thickness of the multilayer with the number of deposition steps. In this system, the main force between the polyelectrolyte molecules is columbic interactions and the structure is stratified [67].

4.2.2 Observation of coated PEI $(PAA/PAH)_n$ on wood by Confocal Laser Scanning Microscopy (CLSM)

CNS results have shown that multilayers composed of PEI $(PAA/PAH)_n$ can be fabricated on wood. However, CNS can only measure bulk systems so it cannot provide evidence for the location of polyelectrolytes in the cellular structure of wood. In order to assist with the determination of polyelectrolyte location adsorbed in wood, confocal laser scanning microscopy (CLSM) was employed to distinguish deposited fluorescence labelled PAH on wood. By utilizing the capability of CLSM to simultaneously detect fluorescence of different wavelengths, FTIC with its specific wavelength was distinguished from the autofluorescence in wood so as to determine the location of PAH.

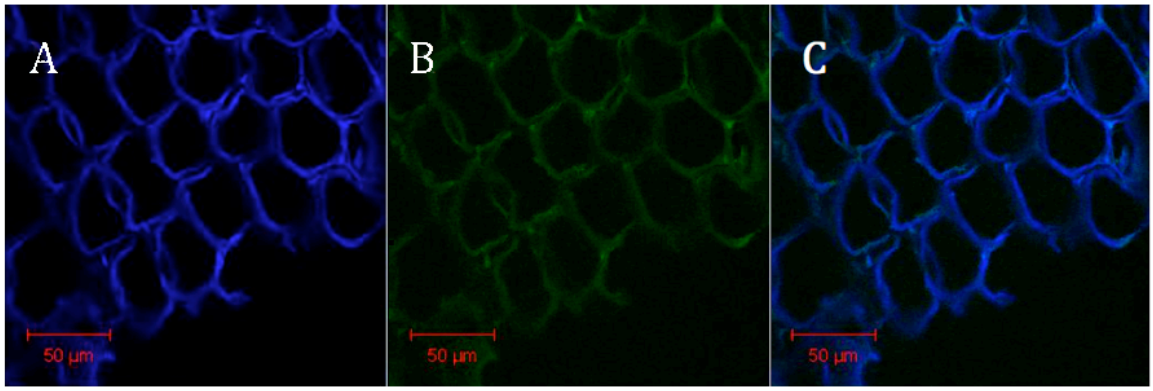

Fig 4.17 CLSM images of bare wood. A) Autofluorescence from wood, λ_{ex}= 364, λ_{em}= 385~470; B) Autofluorescence from wood, λ_{ex}= 488nm, λ_{em}= 505; C) Composite image of A-B.

Fluorescence images of original wood are shown in Figure 4.17. The computer assigned fluorescence blue (image A) and green light (image B) derived from the wood

autofluorescence, which provides detail of the cross section of wood. In the composite image C, green light cannot be distinguished due to its overlap with blue light, except within the cell wall corners in the middle lamella areas.

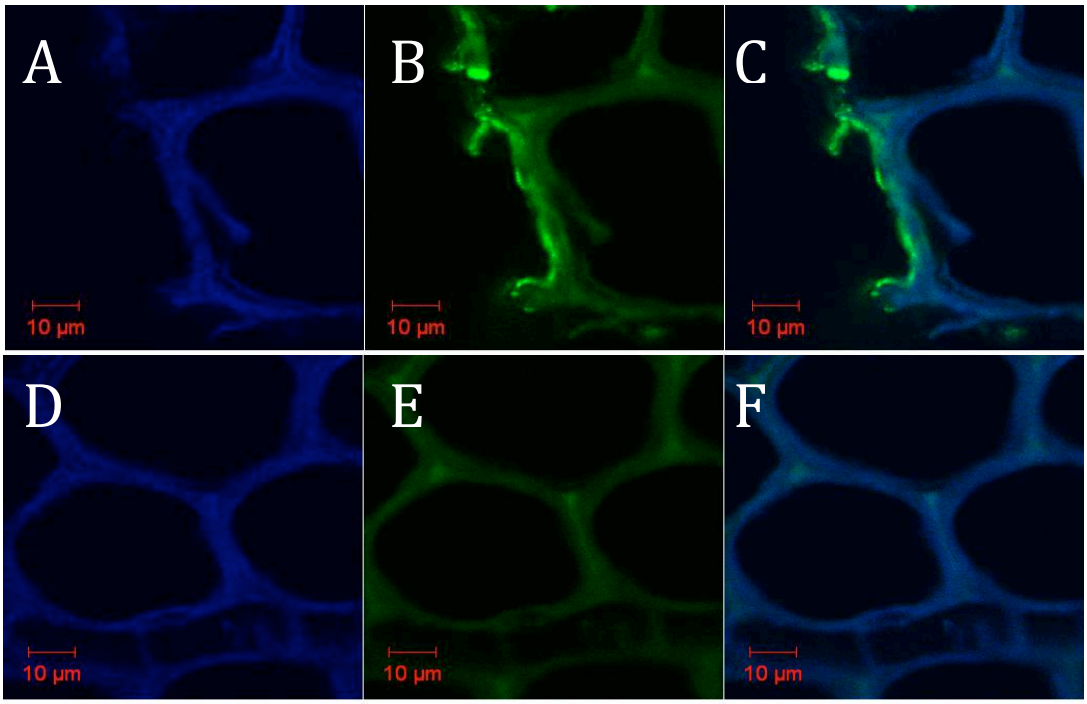

Fig 4.18 PEI $(PAA/PAH)_1$ modified wood. (A-C) Images taken from the edge of the sample; (D-F) Imaged taken from the middle of the sample. A) Fluorescence from autofluorescence in wood, λ_{ex}= 364nm, λ_{em}= 385~470nm; B) Fluorescence from FTIC-PAH and autofluorescence in wood, λ_{ex}= 488nm, λ_{em}= 505nm; C) Composite image of A-B. D) Fluorescence from autofluorescence in wood, λ_{ex}= 364nm, λ_{em}= 385~470nm; E) Fluorescence from FTIC-PAH and autofluorescence in wood, λ_{ex}= 488nm, λ_{em}= 505nm; F) Composite image of D-E.

Fluorescence images of the PEI $(PAA/PAH)_1$ coated wood are shown in Figure 4.18. Images A-C are taken from the edge of a sample section, which demonstrate the coated wood surface. Images D-F are from the interior area, sub-surface region adjacent to the edge, which represents the section of wood not in direct contact to the polyelectrolyte solutions. Fluorescence blue light arising from the autofluorescence in wood is shown in Figure 4.18A&D, similar as the one taken from bare wood sample. The fluorescence light

from PAH is evident in Figure.4.18B, located at the outer border of the first layer of cell wall, shown as bright fluorescence green light. This light has also combined with the green light from the autofluorescence in wood.

FTIC green light with its higher intensity has varying brightness along the cell walls' outer border (figure 4.18B). The varying intensities may result from the confocal method (intensity varies with the fluorescence location in height on the sample), and may also from the different adsorption amounts of polyelectrolyte at different sites of wood surface. The adsorption difference may be attributed to three factors: the heterogeneous morphology of wood surface; defects on the surface resulting from cutting; and the different degree of affinities between PAH and heterogeneous chemical components on the wood surface. In figure 4.18 C, the composited image of A & B, the fluorescence light from PAH becomes more obvious at the edge of wood section and appears continuous, giving evidence that wood surface has been totally covered by the multilayers of (PAA/PAH). As this bright fluorescence light is not observed in the wood sub-surface (Figure 4.18D-F), polyelectrolyte transport appears limited to the outer surface layer. The well arrayed bright green light found in the area of middle lamella (Figure 4.18C) is supposed from wood.

Images taken from the wood samples coated with PEI $(PAA/PAH)_3$ are shown in Figure 4.19, and similar results, as discussed above, are observed in these fluorescence images. The expected intensity increase of fluorescence green light is not found. This may due to the fact that the manipulation of the intensities of fluorescence light by adjusting the focus in confocal method has hidden the slight enhancement of light intensity coming from two nano layer of polyelectrolytes. Figure 4.19 represents the CLSM images taken from PEI $(PAA/PAH)_5$ modified wood samples. The coating still appears similar to images in Figure 4.18 & 4.19, and penetration of PAH into wood cellular structure is also not found. This finding suggests that multilayers composed of PEI and $(PAA/PAH)_n$ are primarily deposited at the top of the outer layer of wood cell walls.

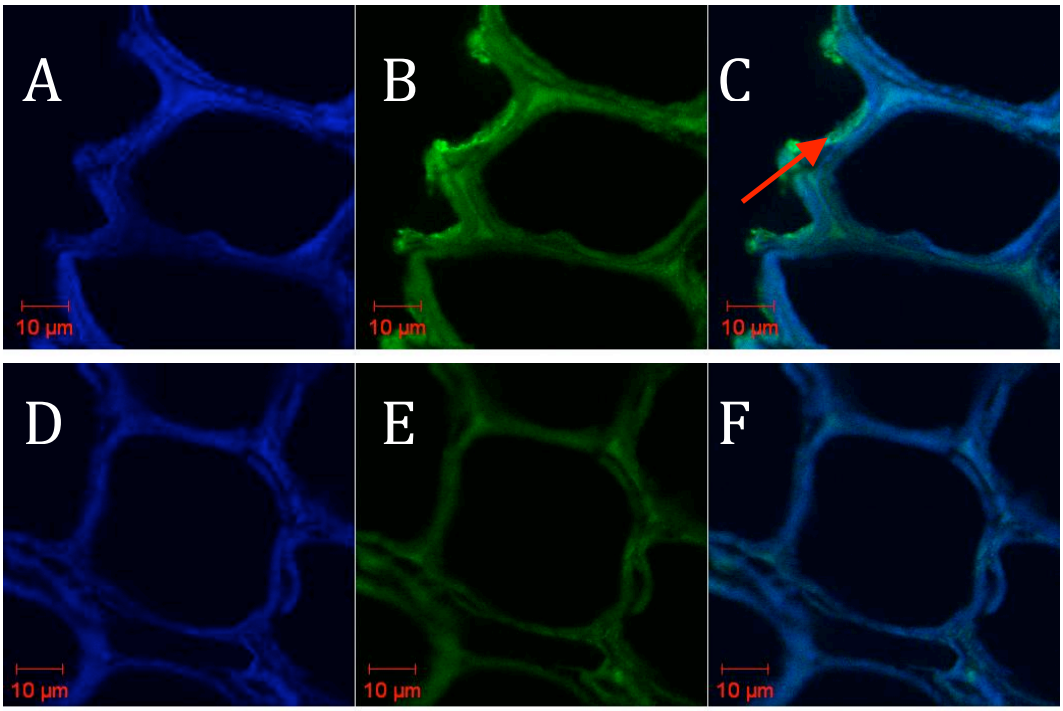

Fig 4.19 PEI $(PAA/PAH)_3$ modified wood. (A-C) Images taken from the edge of the sample; (D-F) Imaged taken from the middle of the sample. A) Fluorescence from autofluorescence in wood, λ_{ex}= 364nm, λ_{em}= 385~470nm; B) Fluorescence from FTIC-PAH and autofluorescence in wood, λ_{ex}= 488nm, λ_{em}= 505nm; C) Composite image of A-B. D) Fluorescence from autofluorescence in wood, λ_{ex}= 364nm, λ_{em}= 385~470nm; E) Fluorescence from FTIC-PAH and autofluorescence in wood, λ_{ex}= 488nm, λ_{em}= 505nm; F) Composite image of D-E.

Penetration of polyelectrolytes into the subsurface of wood through cell walls or pits is not evident, expect for possible cases of where damaged parts of cell walls provide paths for polyelectrolytes go into the subsurface (as white arrow points in Figure 4.20C). It is also observed that at the damaged cell wall edges the fluorescence light is brighter, as the red arrows point in Figure 4.19C and Figure 4.20C. Explanation for this observation is that cut cell walls provide different and increased access to the chemical components on lumen surfaces. Enlarged exposure of microvoids at cut cell wall areas can contribute to the increase of polyelectrolyte adsorption.

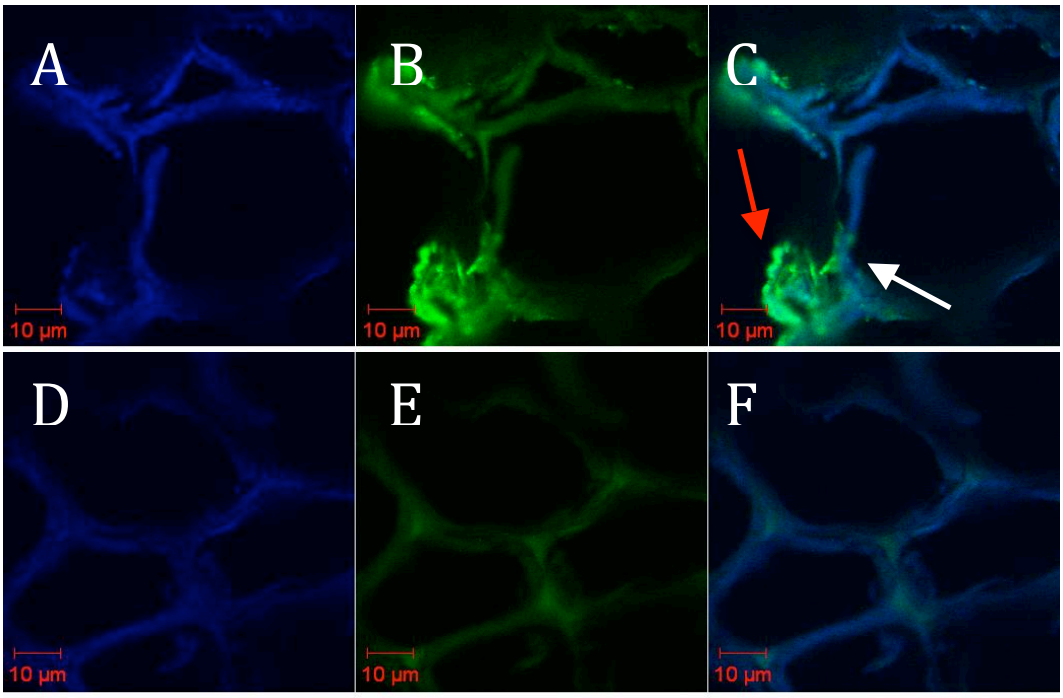

Fig 4.20 PEI $(PAA/PAH)_5$ deposited wood. (A-C) Images taken from the edge of the sample; (D-F) Imaged taken from the middle of the sample. A) Fluorescence from autofluorescence in wood, λ_{ex}= 364nm, λ_{em}= 385~470nm; B) Fluorescence from FTIC-PAH and autofluorescence in wood, λ_{ex}= 488nm, λ_{em}= 505nm; C) Composite image of A-B. D) Fluorescence from autofluorescence in wood, λ_{ex}= 364nm, λ_{em}= 385~470nm; E) Fluorescence from FTIC-PAH and autofluorescence in wood, λ_{ex}= 488nm, λ_{em}= 505nm; F) Composite image of D-E.

4.2.3 Observation of coated PEI $(PAA/PAH)_n$ samples by Environmental Scanning Electron Microscope (ESEM)

CNS provides the quantitative adsorbed amount of polyelectrolytes on wood, while CLSM enables the visualization of fluorescent polymer and also identifies the locations of deposited polyelectrolytes. In this section, an environmental scanning electron microscope is used to visualize the coating on wood. Scanned samples include wood and PEI$(PAA/PAH)_n$ treated wood samples(n=1,5,9). Images in figure 4.21 are taken at 100× magnification covering approximately 1.5 mm^2 of wood area. At this scale, no difference

can be observed between the treated and untreated wood samples. The heterogeneous wood surface structure combined with the microscale wood structure and manipulated mechanical failures are dominant on the surface.

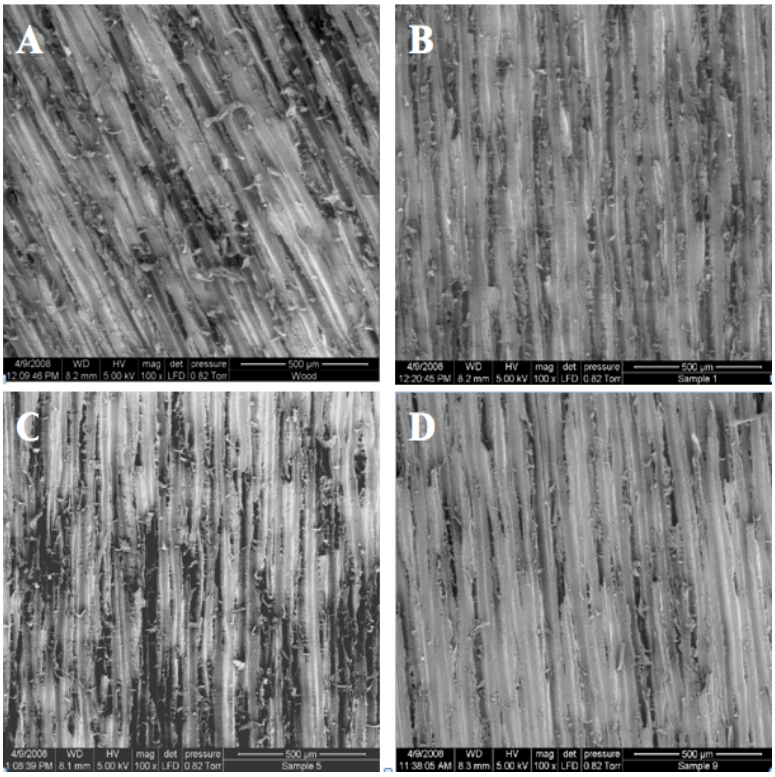

Fig 4.21 ESEM image of wood and wood coated by $PEI(PAA/PAH)_n$ at 100×magnifications. (A) Wood (B) $PEI(PAA/PAH)_1$ coated wood (C) $PEI(PAA/PAH)_5$ coated wood (D) $PEI(PAA/PAH)_9$ coated wood.

When magnification is increased to 2000×, details on the surface of each lumen can be detected and different textures on the wood surface, attributed to the deposited multilayers is observed (Figure 4.22A-D). The cell wall surface of bare wood appears to be relatively smooth with fine fibril texture, except for rough surface of the cut cell walls between lumens, resulting from cell wall damage (Figure 4.22A).

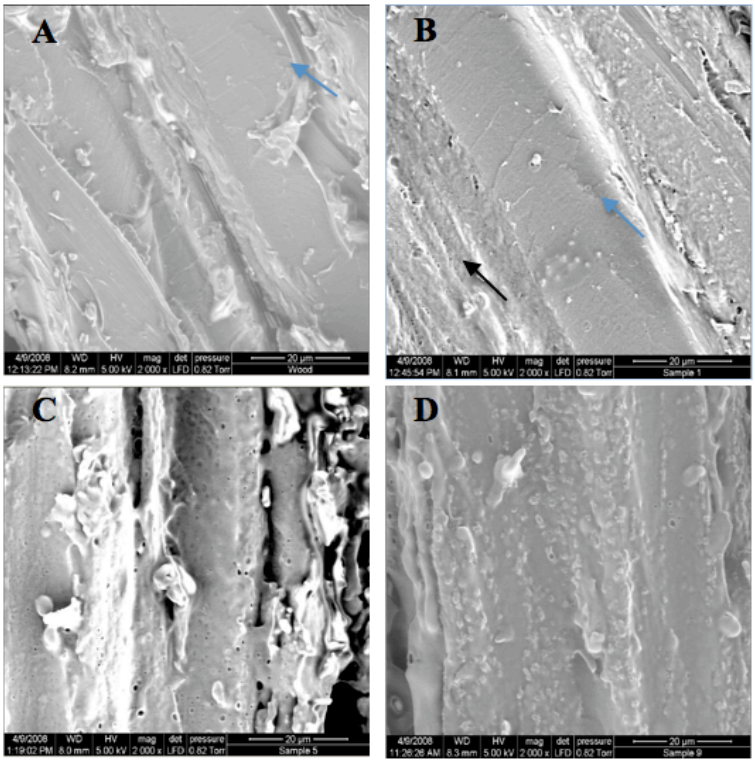

Fig 4.22 ESEM image of wood and wood coated by PEI(PAA/PAH)$_n$ at 2000× magnifications. (A) Wood (B) PEI(PAA/PAH)$_1$ coated wood (C) PEI(PAA/PAH)$_5$ coated wood (D) PEI(PAA/PAH)$_9$ coated wood.

For PEI(PAA/PAH)$_1$ coated samples, corrugated morphology is observed in the cut cell wall structure noted by the black arrow in Figure 4.22B. The former rough areas on the cell wall of lumen appears to be more obvious noted by the blue arrow in Figure4.22A&B. Polyelectrolyte adsorption on the damaged cell wall edge is observed as micron sized clustered or dispersed holes in contrast with the morphology of lumen cell wall area. The aggregation of polymer adsorption at cut cell wall area is in correspondence to the observations from CLSM images where greater adsorption happens at damaged cell wall. The formation of holes is suggested to result from the shrinkage of the multilayers film during the drying process. However, as the number of layers increases to PEI (PAA/PAH)$_5$, due to the increased amount of polyelectrolytes on lumen surface, holes also show on the lumen. Distinct differences of morphology between damaged cell edges and lumen cell surfaces become less obvious as shown in Figure4.22C. In other words, the adsorption difference deriving from the varieties of

wood cell wall structures is less pronounced with the increased layers of PAA/PAH. This finding gives evidence to the former expectation that more polyelectrolytes adsorb to the cut cell wall surfaces first. As the layers keep increasing, morphology of the wood surface almost disappears after the deposition of PEI(PAA/PAH)$_9$, as shown in figure 4.22D. At this time, the coating seems to be more uniform and small extrusions with similar size appear to dominant the surface while the frequency of holes decrease. The reason of having more protuberance with increased number of layers is still unknown but as observed in Figure 4.23C they started to emerge after the adsorption of 5 bilayers of (PAA/PAH).

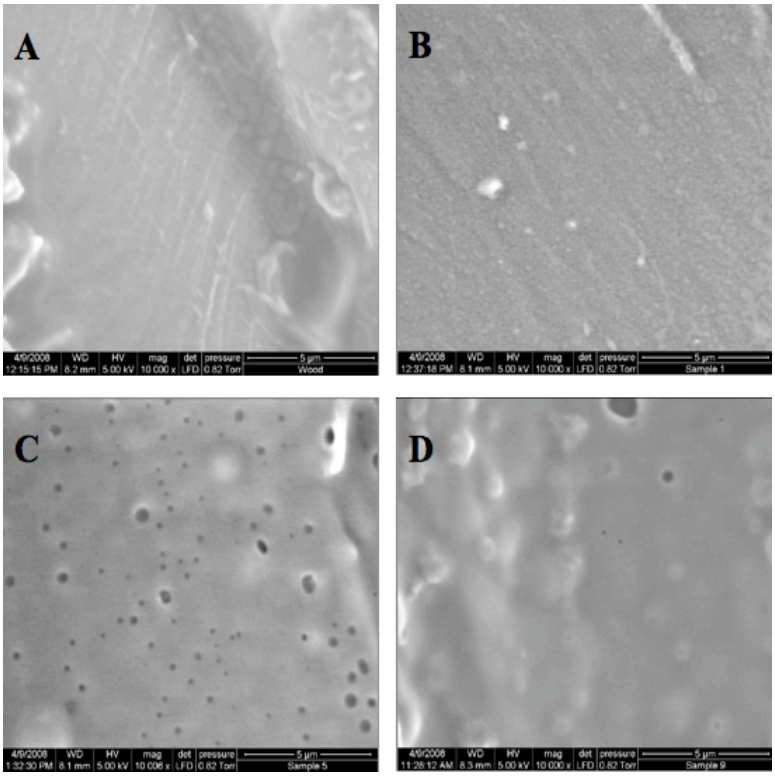

Fig 4.23 ESEM image of wood and PEI(PAA/PAH)$_n$ coated wood at 10K× magnifications. (A) Wood (B) PEI(PAA/PAH)$_1$ coated wood (C) PEI(PAA/PAH)$_5$ coated wood (D) PEI(PAA/PAH)$_9$ coated wood.

The images in figure 4.23 are taken at 10K× magnifications containing one small section of the cell wall lumen surface. In the picture A of untreated wood, fibril nature is still noticeable. While after the adsorption of first three layers of PEI(PAA/PAH)$_1$, the

fibril nature appear to disappear and the surface tends to be uniform and granular(Figure 4.23B). In this stage, the first adsorbed three layers are strongly affected by wood substrates. The diversity of chemical components in the wood cell wall determines that different sites on cell walls have varying degrees of affinities with polyelectrolytes, which afterward results in the unequally adsorption of polyelectrolytes. Hence the formation of grain that are approximately 10^{-1} micrometers in diameter may be related to the various adsorption amounts of polyelectrolytes on different sites of the wood surface. As more polyelectrolytes deposit on the surface, multilayers on the top are free from the influence from substrate and begin to configure on their own. And in this stage protuberant structures start to appear. In Figure 4.23D, the protuberances appear to have an average diameter of 1 μm.

4.3. Substituted spraying for conventional dipping methods

4.3.1 Observation of sprayed one layer of FTIC-PAH on wood by Fluorescence Microscopy

In this section, spraying of polyelectrolytes is studied to fabricate multilayers film on the wood surface, instead of following the conventional dipping methods. After the spraying of polyelectrolytes and water consecutively to the tangential sections, wood specimens with different moisture contents are observed to have FTIC-PAH coated on the surface (Figure 4.24). As the fluorescence images show, when wood is highly hydrated (A&B), polyelectrolyte with bright yellow light (note: the yellow light was assigned by computer) from fluorescence appears to concentrate at the entrance to rays or diffuse into wood through them (Figure 4.24A). As seen in the image from tangential section elliptical bright spots representing the border of rays can be distributed across the tangential surface (Figure 4.24B).

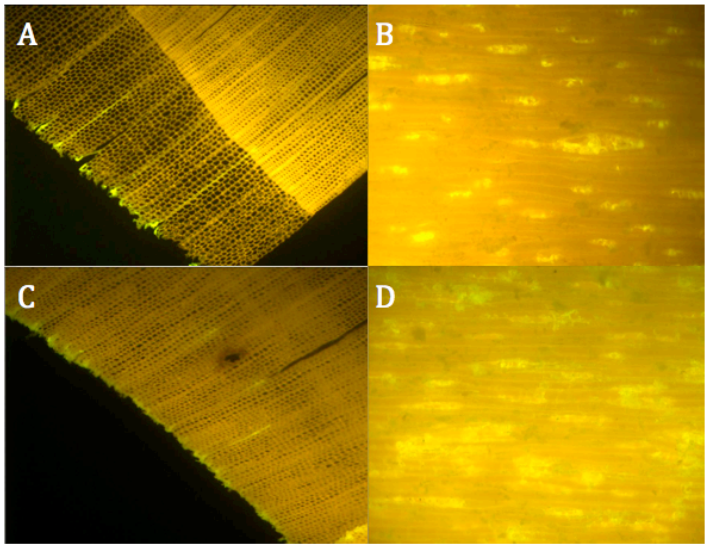

Fig 4.24 One layer of FTIC-PAH coated wood. A&B) images taken from water soaked wood samples; C&D) images taken from conditioned samples.

For the wood samples that were stored in conditioning chamber prior to treatment, which means the moisture content is around 10%, the coating no longer traces the outline of rays. As Figure 4.24D shows, the areas of fluorescence light spots on wood surface are extended outside the ray cells and appear to have no regular shape, indicating more adsorbed PAH. This change is also reflected in the cross sectional images that continuous

coating of polyelectrolytes is observed at the edge of wood section (Figure 4.24C). Rays function as horizontal transport of liquid, so they are likely candidates to allow movement of polyelectrolyte into the subsurface of wood. Though some low molecular weight polymer may penetrate through pits in the connections of lumens or even cell walls, in this case, PAH (molecular weight of 15,000) does not show transfer. Therefore it is shown in the fluorescence images that in the areas where there are longitudinal tracheids, polyelectrolytes are observed to stay mostly on the first layer of lumen.

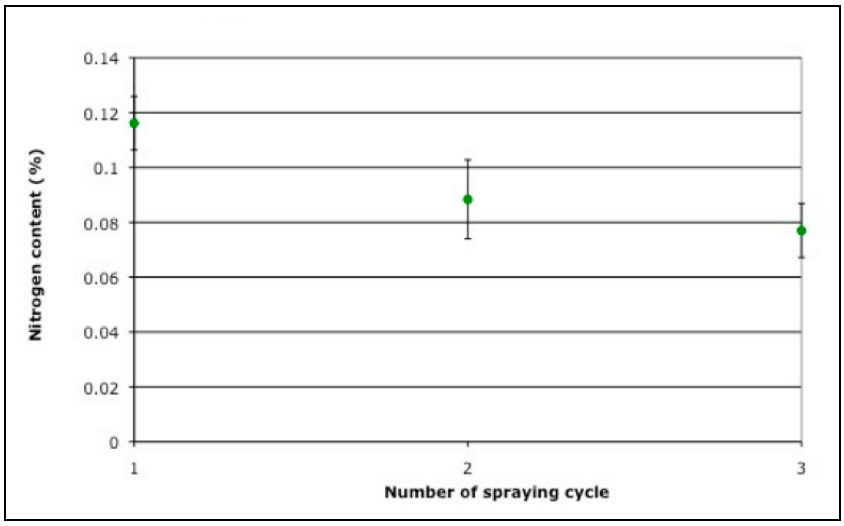

Fig 4.25 Nitrogen contents in wood samples that have been sprayed by PAH and PAA consecutively. One cycle contains the spraying of (PAH/water/PAA/water). Average values were taken from 3 measurements. Error bars represent ±1 standard deviation.

The absence of consistent deposited polyelectrolytes on the surface of lumen cell wall of hydrated wood is not clearly known, but similar result is found in CNS measurements of wet wood samples that have been sprayed of oppositely charged polymer in cycles. Instead of obtaining increased amount of polyelectrolytes on wood, decreases are observed (Figure 4.25), indicating the failure of coating a consistent primer layer on wood the first time. It is suspected that the failure is due to the limitation of diffusion of the polyelectrolyte to the wood surface as the excess polyelectrolyte drips off when wood flake samples are placed vertically. And the optimization data (Figure 4.15) shows the polyelectrolyte needs to be in excess to achieve optimal adsorption.

4.4 Detection of cross-linking between PAH and PAA in multilayer after heat treatments

4.4.1 Observation of PEI $(PAA/PAH)_n$ on silicon substrates

4.4.1.1 FTIR spectra of PAA and PAH cast films

An FTIR spectrum of PAA is shown in Figure 4.26 and its major vibration modes are listed in Table 4.1. The absorbance peak of C=O (1711 cm^{-1}) from carbonyl (–COOH) in PAA is observed, while the asymmetric stretching peak of the carboxylate ($–COO^-$) at ν=1565-1543 cm^{-1} is not noticeable [76]. Absence of carboxylate peak should result from the condition PAA cast film is prepared, where pH of the aqueous solution is below 3 and PAA still exists in its nonionized form. Spectrum of PAA cast film that has been heated at 250°C for 2 hours is also displayed in Figure 4.26. As the spectrum shows, except for the original signals, a minor change is found as one more peak appears at the 1803 cm^{-1}, which is associated to the formation of anhydride bonds from COOH groups [82].

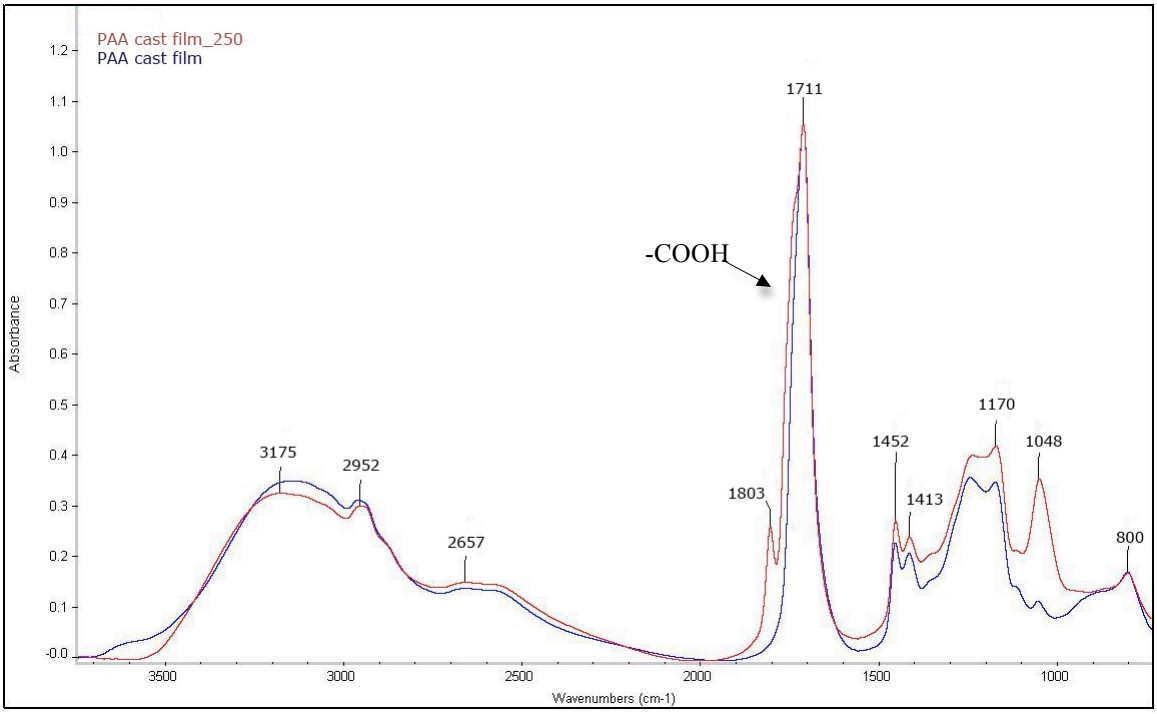

Fig 4.26 Comparison of FTIR spectra of PAA cast film before and after 2h heating at 250°C in transmission mode.

Table 4.1 Infrared bands of PAA

Band Position in cm^{-1}	Assignments [82]
3175	O-H stretching
2952	asymmetric CH_2 stretching
2500~2700	Overtones and combinations of bands near 1413 and 1248cm^{-1} enhanced by Fermi resonance
1711	C=O stretching
1452	CH_2 deformation
1413	C-O stretching coupled with O-H in-plane bending
1170	C-O stretching coupled with O-H in-plane bending

FTIR spectrum of PAH cast film before and after heat treatment is shown in Figure 4.27, and its major vibration modes are listed in Table 4.2. It is observed that most chemical groups in PAH do not change after 2 hour heating at 250°C, except for the peak at 3388 cm^{-1} associated with O-H stretching shown after heat treatment.

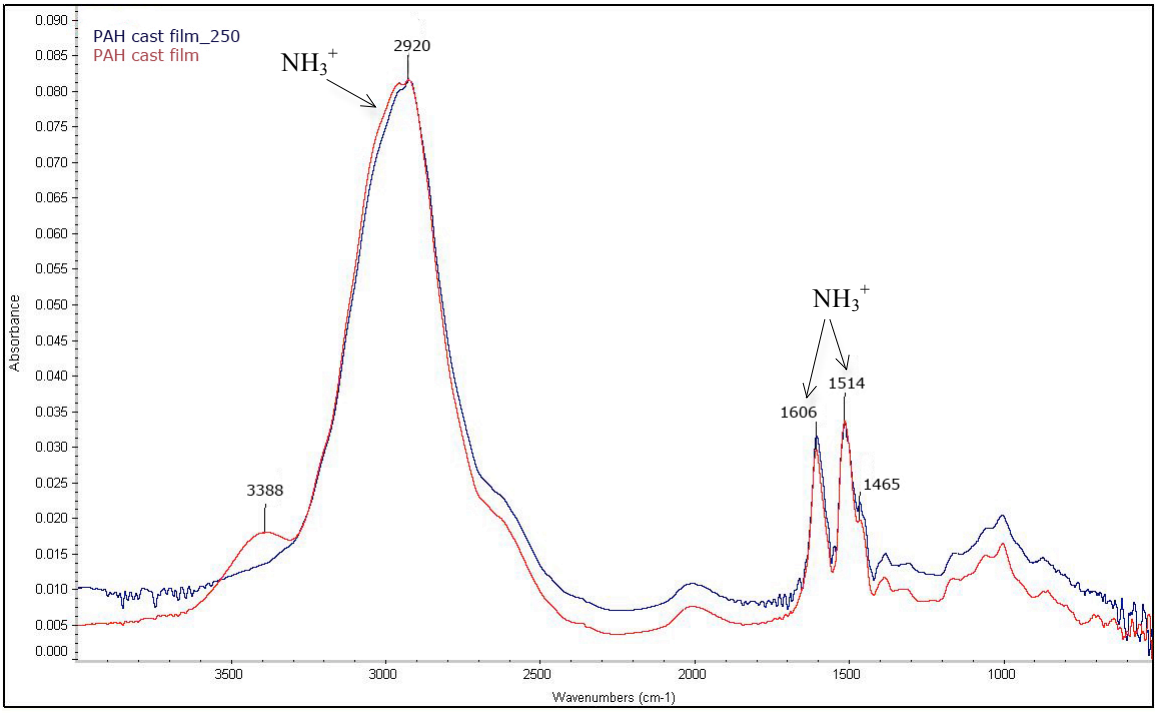

Fig 4.27 Comparison of FTIR spectra of PAH cast film before and after 2h heating at 250°C in transmission mode.

Table 4.2 Infrared bands of PAH

Band Position in cm^{-1}	Assignments [76]
3388	O-H stretching
3016	asymmetric NH^{3+} band
2920	asymmetric CH_2 stretching
1606	asymmetric NH^{3+} band
1514	symmetric NH^{3+} band
1465	CH_2 deformation

4.4.1.2 FTIR spectra of PEI $(PAA/PAH)_n$ multifilms

The thickness of one layer of PAA or PAH is around 3~5nm when they are formed under the pH of 6~7 [67]. Therefore, the signals for a few layers deposited on the surface are very weak and the spectrum is mainly dominated by noise. Experimental results show that only when the number (n) of bilayers (PAA/PAH) reaches 9, can peaks for each molecular group be clearly identified (Figure 4.28). Though noise exists in the FTIR spectra taken from multifilms with less number of layers, increase of absorbance can still be observed as a function of growing number of bi-layers, which changes from -0.005 to 0.02 when n increases from 1 to 9. The increase of absorbance as a result of the increment in the number of layers on the surface suggests the fabrication of multilayers of $PEI(PAA/PAH)_n$ on the silicon substrate because of the Beer-Lamebr law.

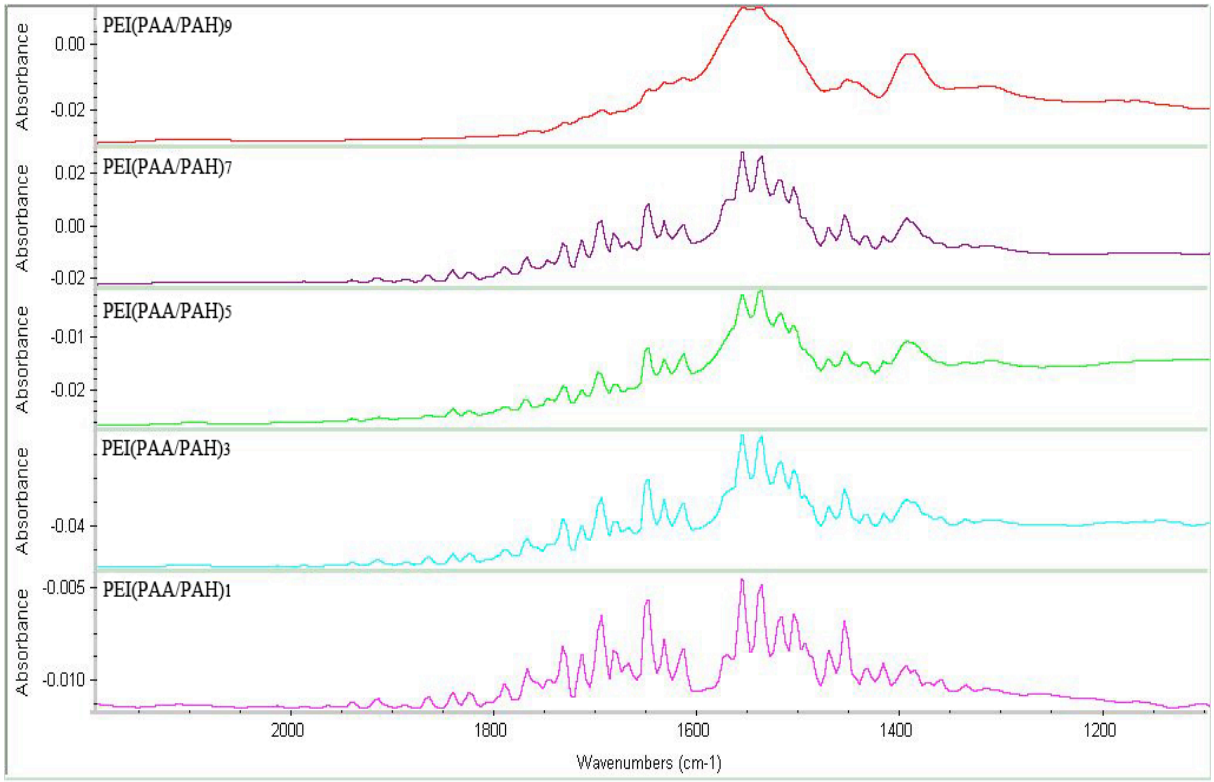

Fig 4.28 FTIR spectra of PEI(PAA/PAH)$_n$ multifilms (n=1,3,5,7 & 9) on silicon substrate in transmission mode.

It has been reported that the acid groups of PAA are up to 80% ionized at pH 7 [76]. This phenomenon has been observed in this study as shown in the FTIR spectra of multilayer films composing of PEI (PAA/PAH) $_9$ which were rinsed with Milli-Q water at pH 7(Figure 4.29). The major vibration modes are listed in Table 4.3. As data shows, the absorbance intensity of –COOH (1692^{-1}) is weakened dramatically as most of carboxyls have become ionized, and the signals for $–COO^-$ are clearly enhanced. The symmetric and asymmetric stretches of $–COO^-$ can be attributed to peaks 1391 cm^{-1} and 1549 cm^{-1} respectively [76]. The N-H bending from PAH can be assigned to the peak at 1606 cm^{-1}. In the region from 4000 to 2000 cm^{-1}, the peak at 2923 cm^{-1} can be assigned to CH_2. The peaks for NH_3^+ (3016 cm^{-1}) and O-H (3140 cm^{-1}) stretching are overlapped by CH_2 and can be detected at its shoulder [76,82].

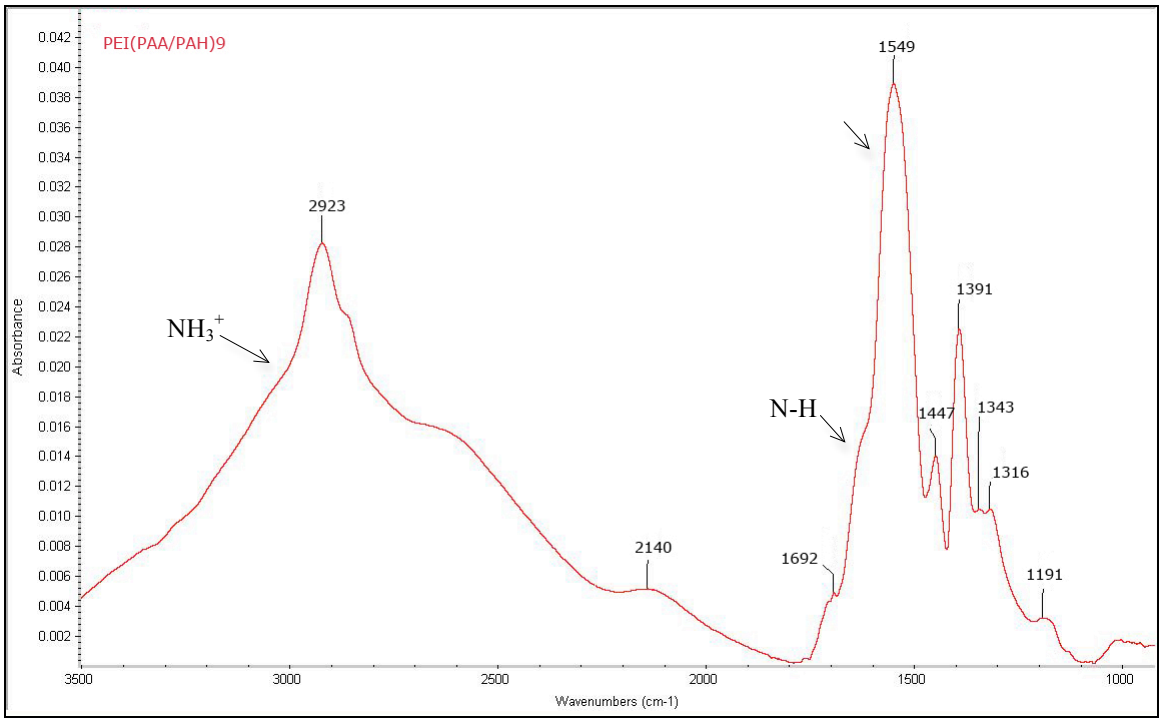

Fig 4.29 FTIR spectra of PEI(PAA/PAH)$_9$ multilayer film on silicon substrate in transmission mode.

Table 4.3 Infrared bands of PEI(PAA/PAH)$_9$ multilayer film

Band Position in cm^{-1}	Assignments [76,82,83]
2923	asymmetric CH_2 stretching
2500~2700	Overtones and combinations of bands near 1413 and 1248cm^{-1} enhanced by Fermi resonance
1692	C=O stretching
1606	asymmetric NH^{3+} band
1549	asymmetric $–COO^-$ stretch
1447	CH_2 deformation
1391	symmetric $–COO^-$ stretch
1343	C-H stretching

4.4.2 Detection of cross-linking between PAA and PAH

Previous work has shown that ammonium group of PAH and carboxylate group of PAA can be cross-linked via amide bonding by heating for 2 hours at 130°C or half an hour at160°C [42-44]. In this study, multilayers film of PAA and PAH was first heated at 250°C in a conventional oven for 2 hours. The FTIR spectrum of the heated multilayer film is shown in figure 4.30. The amide peak appears at 1671cm^{-1}, indicating the formation of amide linkage between PAA and PAH [42]. Another amide peak around 1550 cm^{-1} may have overlapped with the signal from carboxylate and can be seen at 1549 cm^{-1} [43]. Absorbance peaks of carboxylic acid and carboxylate groups of PAA, and N-H bending from PAH was dramatically decreased, but still noticeable, suggesting that the cross-linking was incomplete after heating at 250°C for 2h.

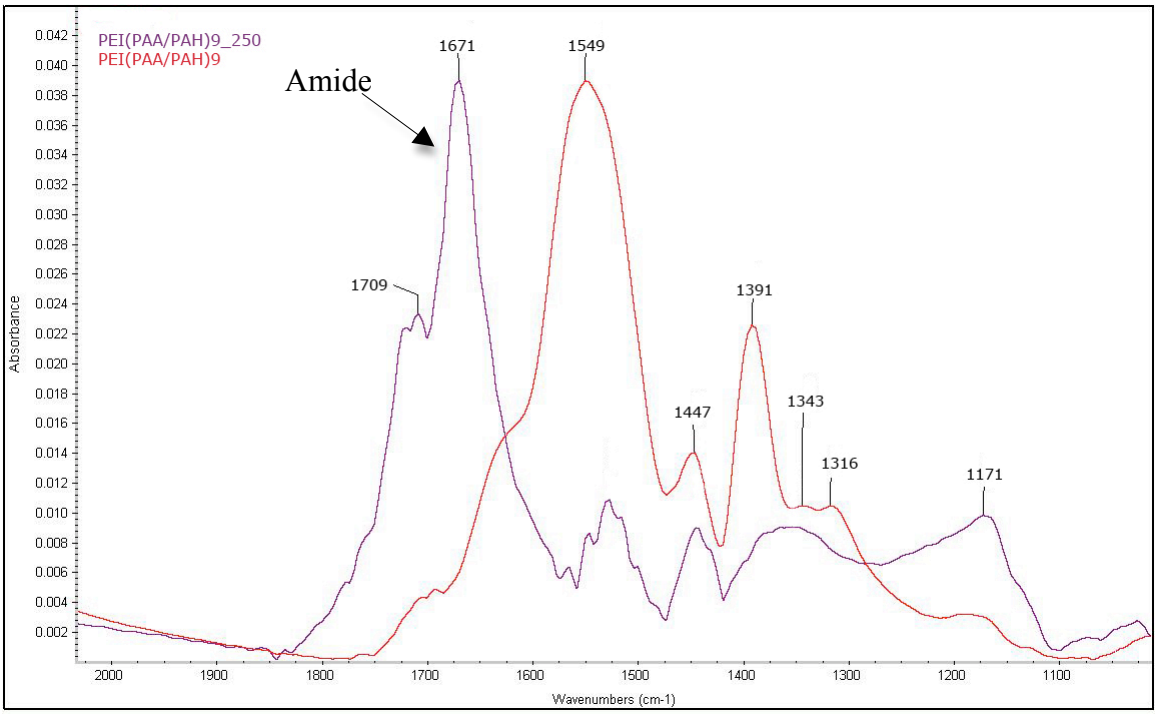

Fig 4.30 Comparison of FTIR spectra of PEI(PAA/PAH)$_9$ multilayers film before and after 2h heating at 250°C in transmission mode.

To detect the influence of temperature on cross-linking, multilayer films of PEI (PAA/PAH)$_{15}$ were prepared and heated at a range of temperatures for 2h. The peak related to amide bond formation at 1671cm^{-1} was first seen in the spectra for the

multilayers film that was heated at 150°C. As the temperature increased, absorbance intensity of amide bond also increased, suggesting more extensive cross-linking at higher temperatures (Figure 4.31 & 4.32). The multilayers films were also heated at constant temperatures for a series of time range (1/2, 1, 2 and 4h), to examine the influence of time on the formation of amide bond. Results from FTIR spectrum indicates that it takes at least 2h to achieve detection of the amide bond, and extended heating time of 4 hours does not lead to any change in the intensity of the amide peak.

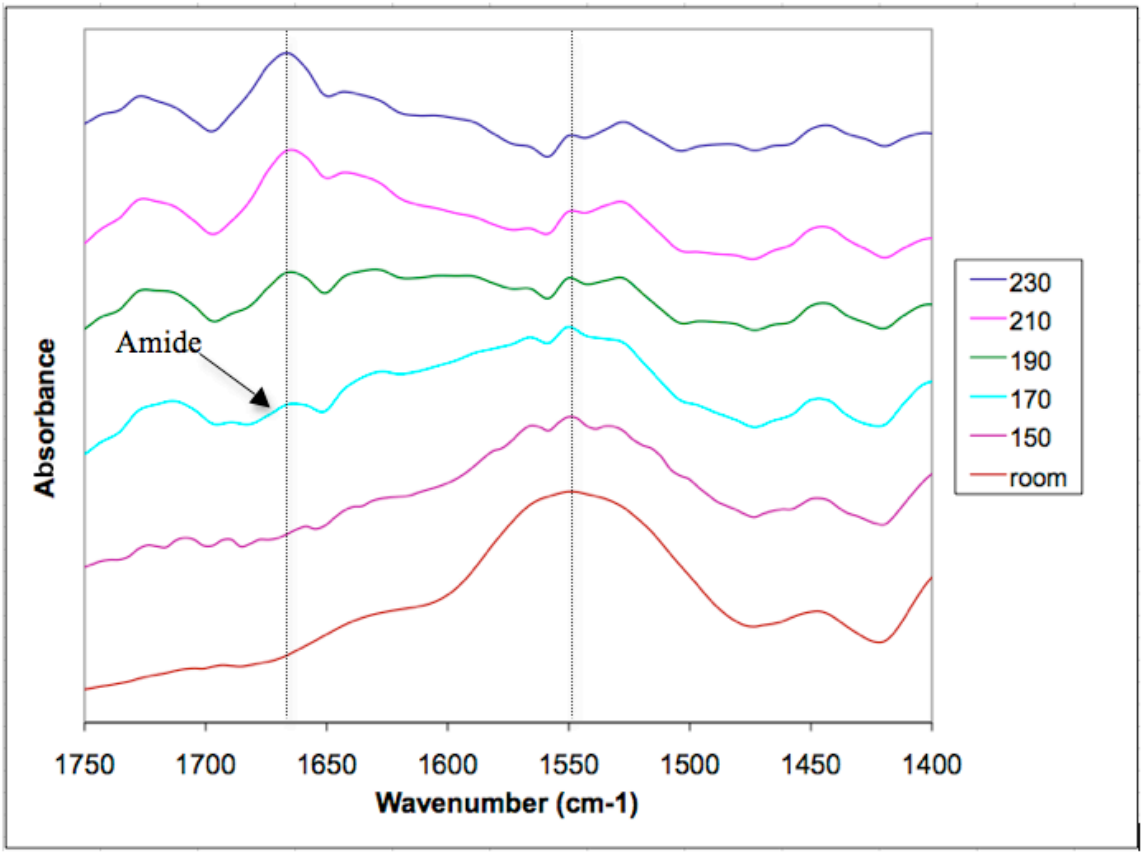

Fig 4.31 FTIR spectrum of cross-linking between PAA and PAH after the multilayers films were heated in a range of temperature for 2h.

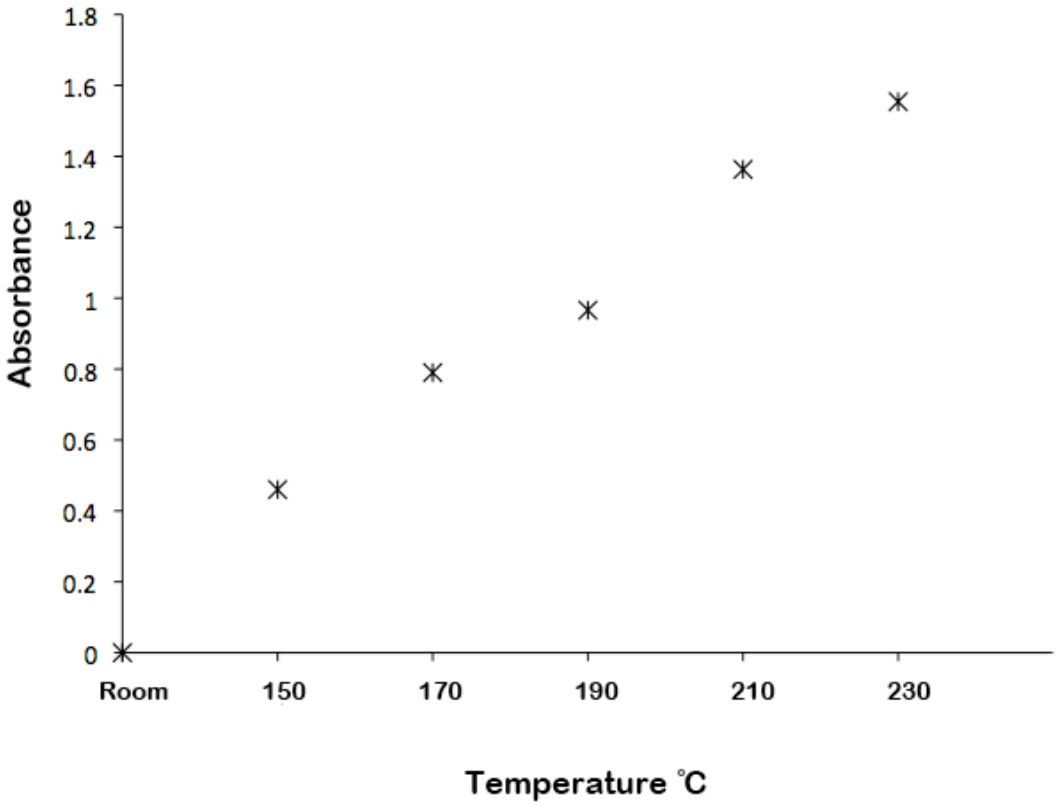

Fig 4.32 Absorbance intensity of amide bond as a function of heating temperature at wavenumber of 1671cm^{-1}.

4.5 Mechanical testing

4.5.1 ASTM D905 test for strength properties in shear by compression loading

Wood strips coated with multilayer of PEI(PAA/PAH)$_9$ can be bonded together in a hot press when one strip has PAA as terminal coated layer and the other has PAH. This can be achieved with a temperature of 100°C, pressure of 300psi and a time period of a half hour. However, no chemical bond or cross-linking has been formed between PAA and PAH at this temperature. While the bonded strips cannot be pulled apart, as they are soaked in water, dimensional changes occur, and they easily break apart. Extended the time to 1 h does not make obvious changes to the results. However, as the core temperature is elevated to 150°C, samples that have been bonded for both ½ and 1h pressing time remain intact upon exposure to moisture, and even under severe exposure of 2h in boiling water. The attained water-resistant property in bondline should be attributed to the changes in the interaction between the polyelectrolytes and polymeric materials in wood. This finding is corresponding to the results obtained from FTIR experiments, where 150°C is the initial temperature to have cross-linking between PAA and PAH.

To investigate the relationship between the number of layers and bonding strength provided by multilayers film, compression shear tests are performed following the ASTM D905 standard with minor deviation of the sample dimension. Phenol formaldehyde (PF) and mixture of PAA and PAH were also tested in order to compare the performance of the commercially used adhesive for wood composite with LBL system, and simply blending of polyelectrolytes with well designed LBL assembly. Similar amounts of PF or physical mixture to the approximated total amount of polyelectrolytes on multilayers film that has 18 bilayers are applied.

Results show that in the range of estimated bondline thickness from around 108 to 180nm (one layer is about 3~5nm), the shear strength of multilayer bonded specimens increase as a function of the number of layers (Figure 4.33). PF exhibits relatively higher shear strength than LbL system when they have equal solid contents, while the mixture of PAA and PAH is the weakest although it contains the same amount of polyelectrolytes as the one the sample with 18 bilayers. Shear strength of all the specimens tested wet

lowered after weathering, but still kept the same trend with respect to the relationship between shear strength and resin types. When comparing LbL assembly films versus mixed films, the polymer distribution on the surface and the nanoscale organization are the two main differences that could account for the increased strength of the multilayers film. The difference is highlighted in the weathering tests where the mixture of PAA and PAH cannot resist the stress released from the wood strips during dimensional changes in the condition room and fail apart before the boiling test.

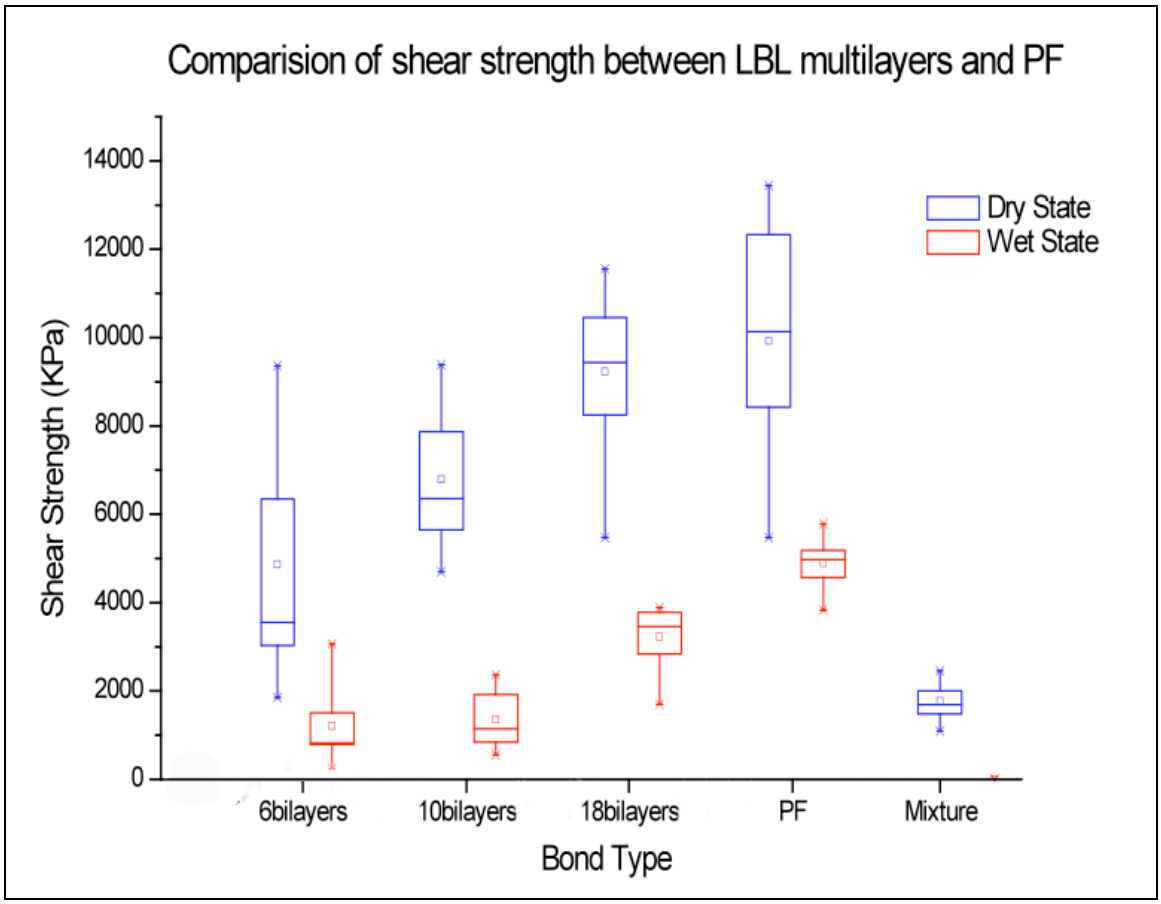

Fig 4.33 Shear strength of multifilms with different numbers of bi-layer in the bondline, PF and mixture of PAA and PAH under both dry and wet conditions.

Shear blocks that contain 18 bilayers of polyelectrolyte in the bondline appear to have the highest wood failure, followed by PF, 10 bilayers and 6 bilayers of polyelectrolytes. No wood failure is found in the blocks that are bonded by the mixture of PAA and PAH (Figure 4.34). The great amount of wood failure near the bondline from 18 bilayers and

PF samples may result from the penetration of bonding materials into wood and the formation of strong bonding in the bondline area. It is known that adhesives, especially the ones that have low viscosity and molecular weight, can penetrate into wood through its lumens, pits, and even the cell wall as they are applied to the surface [77]. Tarkow et al. (1966) has studied the penetration of polyethylene glycol (PEG) into wood and obtained a critical molecular weight of 3000 to penetrate through the cell wall. And this value can be larger given higher temperature. As found in the study of UF for beech (Sernek et al.1999), with assistance of external pressure, the adhesive penetration can be ten times larger than the one obtained when no force was applied.

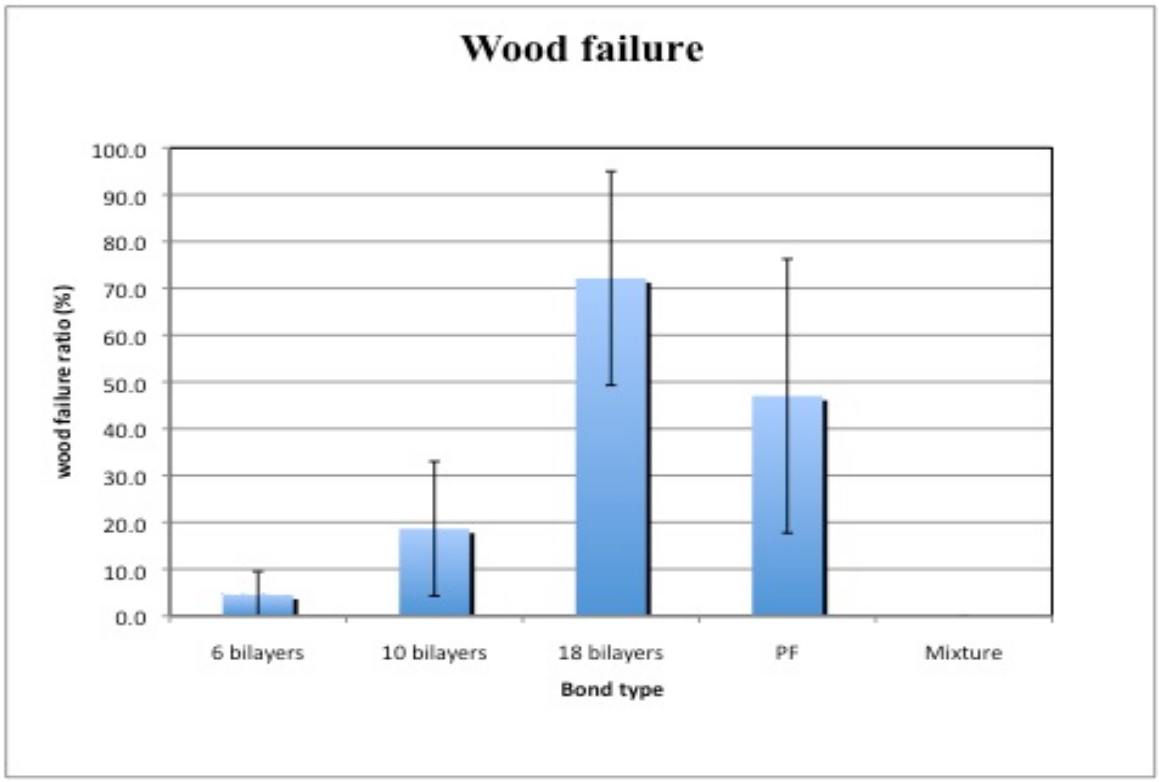

Fig 4.34 Wood failure from shear lap blocks that contain different numbers of bi-layers of polyelectrolytes, PF and mixture of PAA and PAH in the bondline. Average values were taken from 14 measurements. Error bars represent ±1 standard deviation.

Hence, in this research PF is possible to penetrate the lumens through pits and cell wall under both high pressure and high temperature. While polyelectrolytes with molecular weight of 25,000 (PEI), 100,000(PAA) and 70,000 (PAH) may not penetrate

through the cell wall, especially for the multilayers films that are ionically inked together. Given high temperature, the penetrated polymers may cross-link and reinforce the wood, whereupon making the wood in the bonded area stronger than the pure wood. As wood failure was high for both 18-bilayer and PF specimens, the shear strength obtained may not represent the true properties of the bonding but the shear strength of wood. Therefore, the comparison of LbL system with PF by their shear strength values becomes questionable. As to the blocks that contain only 6 or 10 bilayers of polyelectrolyte, there is not sufficient polymer present on the wood surface to provide the stress transfer. Either the microstructure of wood prevents intimate contact or thin multilayer films do not have the inherent strength to carry the load. The mixture cannot provide as strong bonding as the LBL system, so the bondline failure always happen. It is interesting to note that even 180nm thick bondline is below the surface height topology of the wood surface. The suggested size for the adhesive to be thick enough to bridge the microstructure may not be a universal requirement for bonding wood if the resin is perfectly distributed across the surface.

CHAPTER 5 – CONCLUSIONS

Wood based composite performance is influenced by adhesive type and adhesive amount. A novel method to coat wood substrates was investigated to: 1) investigate the effect of solution parameters, pH and ionic strength, on the formation of multilayer films on wood; 2) determine the influence of wood cellular structure on the formation of multilayer films on wood; 3) determine the ability to use spraying deposition as a method of multilayer film fabrication on wood; and 4) measure the shear strength of shear blocks that have been bonded together under the hot press, after they have been coated with multilayers.

As to objective #1:

For solution with high pH values, zeta potential of the wood particles increased in magnitude and became more negative.

Solution pH had a positive effect on the adsorption of PEI and PDDA on wood particles as the first layer, given constant ionic strength.

Salt ions competed with PEI or PDDA for the charged sites on the wood surface and had a negative effect on the adsorption of PEI and PDDA on wood particles. The decrease of adsorption of polyelectrolytes with the presence of salt was also attributed to the screening of the surface charge on polyelectrolytes by salt, which led to the decrease of coulombic static attraction between polyelectrolytes and wood surfaces.

Objectives #2:

When PAH with molecular weight of 15,000 were applied to the tangential sections of wood samples, diffusion of polyelectrolytes into wood through pits or lumen cell walls of southern yellow pine did not occur, while penetration through the rays having simple pits was numerous. Increase of bi-layers of (PAA/PAH) on wood substrates did not influence the transport through border pits or lumen cell walls either. Based on SEM analysis of coated wood, multilayers film formation was effected by the wood substrates when less then 3 bilayers were applied and more adsorption of polyelectrolytes happened on the cut lumen wall surface. As the number of layers increased, the influence from wood decreases.

Objectives #3:

In this project, utilization of spraying for LbL technique did not achieve the fabrication of multilayer films on wood as detected by CNS analysis. Fluorescence images of adsorbed PAH showed higher adsorption of PAH on the wood samples that were stored in conditioning room prior to treatments than the ones soaked in the water. When wood was fully hydrated, PAH only adsorbed on or penetrated through rays. When the moisture content of wood decreased to around 10%, adsorption on both lumen cell walls and rays was observed.

Objectives #4:

Wood strips coated with multilayer of PEI(PAA/PAH)$_9$ could be bonded together under the hot press, at 100°C and 300psi for half hour, without the cross-link between PAA and PAH. Under the same pressure and pressing time, and increasing the temperature to 150°C achieved water stable bonds. This initial temperature for cross-link is lower that the one measured from the multilayer films coated on silicon substrate, which is 190°C.

Compression shear tests showed the bonding strength provided by multilayer films in shear blocks increased as a function of the number of layers. PF exhibited relatively higher shear strength than LbL system given the equal solid contents on the wood substrates, while the controlled physical mixture of PAA and PAH is the weakest although it contains the same amount of polyelectrolytes as the sample with 18 bilayers. Shear strength of all specimens decreased after weathering, with the same trend with regard to the relationship between shear strength and resin types.

Shear blocks that contain 18 bilayers of polyelectrolyte in the bondline appear to have the highest wood failure (70%) followed by PF (50%), 10 bilayers (20%) and 6 bilayers (5%) of polyelectrolytes. No wood failure was found in the blocks that are bonded by the mixture of PAA and PAH, and for all wet specimens. Large wood failure ratio from 18 bilayers and PF samples gave evidence that the measured shear strength might actually represent the shear strength of wood and not LbL multilayer films or PF performance.

Future work should involve testing of the adhesives using an energy approach to determine adhesive performance.

In summary, LbL assembly can be used to build films on wood substrates that are thinner than the microscale elements on wood substrates, providing a route towards surface functionalization that minimizes polyelectrolyte loading.

REFERENCE

[1] Larsson A, Kuckling D and Schonhoff M 2001 Colliod Surf. A 190 185-92.

[2] Schonoff M, Larsson A, Wellzel P B and Kuckling D 2002 J. Phys. Chem. B 106 7800-8.

[3] Shimazaki, Y., Mitsuishi, M., Ito, S., Ymamoto, M., Langmuir 1997, 13, 1385-1387.

[4] Serizawa, T., Hashiguchi, S., Akashi, M., 1998 Langmuir, 15, 5363-5358.

[5] Serizawa, T., Akashi, M., 1998 J. Polym. Sci., 37, 1903-1906.

[6] Decher, G., Schmitt, J., Siegmund, H. U., Heiliger, L., 1995 Eur. Pat. EP 647 477 A1.

[7] Pearson, C., Nagel, J., Petty, M.C., 2001 J. Phys. D, Appl. Phys., 34, 285-291.

[8] Serizawa, T, Hamada, K., Kitayama, T., Katsukawa, K., Hatada, K., Akashi, M., 2000 Langmuir, 16, 7112-7115.

[9] Decher, G., Lehr, B., Lowack, K., Lvov, Y., Schmitt, J., 1994 Proteins or DNA, Biosens, 9, 677-684.

[10] Ladam, G., Schaad, P., Voegel. J. G., Schaaf, P., Decher, G., Cuisinier, F., 2000 Langmuir, 16, 1249-45.

[11] Sukhorukov G B, Donaath E, Lichtenfeld H, Knippel M, Budde A and Mohwald H 1998 Colloid Surf. A 137 253-66.

[12] Donath E, Sukhorukov G B, Caruso F, Davis S A and Mohwald H 1998 Angew. Chem. Int. Edn 37 2202-5.

[13] Iler, R.K.. Multilayers of Colloidal Particles, 1996 J.Colloid Interface Sci., 21, 569-594.

[14] Decher G, Hong J D and Schmitt J 1992 Thin Solid films 210 831-5.

[15] Decher, G., 1997 Science, 277, 1232-1237.

[16] Decher,G, Hong J.D, Makromol. 1991 Chem. Macromol. Symp., 46, 321

[17] Schlenoff, J.B.; Dubas, S.T. 2001Macromolecules, 34, 592

[18] Stephan T., Dubas and Joseph B. Schlenoff, 2001Langmuir, 17,7725-7727

[19] Ruths J, Essler F, Decher G and Riegler H, 2000Langmuir, 16, 8871-8

[20] G. Ladam, P. Schaad, J.C. Voegel, P. Schaaf, G. Decher, and F. Cuisinier, 2000Langmuir, 16, 1249-1255

[21] Harris, J. J.; Bruening, M. L. 2000Langmuir, 16, 2006

[22] Mendelsohn, J. D., Barrett, C. J., Chan, V. V., Pal, A. J., Mayes, A. M., & Rubner, M. F., 2000 Langmuir, 16(11), 5017-5023.
[23] Schlenoff, J. B., Dubas, S. T., & Farhat, T., 2000 Langmuir,16(26), 9968-9969.
[24] Izquierdo, A., Ono, S. S., Voegel, J. C., Schaaff, P., & Decher, G., 2005 Langmuir, 21(16), 7558-7567.
[25] Michel, A., Izquierdo, A., Decher, G., Voegel, J. C., Schaaf, P., & Ball, V., 2005 Langmuir, 21(17), 7854-7859.
[26] Meiwen Cao, Jinben Wang, Yilin Wang, 2007 Langmuir, 23, 3142-3149
[27] Stephan T. Dubas, Joseph B. Schlenoff, 2001 Langmuir, 17, 7725-7727
[28] Lingstrom Rikard, Wagberg Lars, Larsson Per Tomas., 2006 J.Colloid Interface Sci, 296,2 396-408
[29] Donath E, Walther D, Shilov VN, et al., 1997Langmuir, 13, 5294-305.
[30] Schwarz B, Schonhoff M., 2002Coll Surf a-Physicochem Eng Aspects, 198, 293-304
[31] Abe, H., Funada, R., Kuroda, N., Furusawa, O., Shibagaki, M., & Fujii, T., 2001 Iawa Journal, 22(1), 63-72.
[32]Dill-Langer, G., Lutze, S., & Aicher, S., 2002 Wood Science and Technology, 36(6), 487-499.
[33] Knebel, W., & Schnepf, E., 1991 Trees-Structure and Function, 5(1), 1-4.
[34] Li, K. C., & Reeve, D. W., 2005 Cellulose Chemistry and Technology, 39(3-4),211-223.
[35] Matsumura, J., Yamasaki, Y., Oda, K., & Fujisawa, Y., 2005 Journal of Wood Science, 51(4), 328-333.
[36] Mislankar, A., Darabie, A., & Reeve, D. W., 1997 Journal of Pulp and Paper Science, 23(2), J73-J76.
[37] Xiao, Y., Kreber, B., & Breuil, C., 1999 International Biodeterioration & Biodegradation, 44(4), 185-190
[38] Donald A.M., 2003 Nature Materials, 2, 8, 511-516
[39] Stokes D.J., 2003 Philosophical Transactions of the Royal Society of London Series A-Mathematical Physical and Engineering Science, 361, 1813, 2771-2787
[40] L. Daniliuc, C. Kesel & C. David., 1992 Eur. Poly. J., 28, 11, 1365-1371
[41] Guocheng Yang, Jian Gong, Rui Yang, Hongwei Guo, Yizhe Wang, Baifeng Liu & Shaojun Dong, 2006 Electrochemistry Communications, 8, 790-796

[42] Jeremy J. Harris, Paul M. DeRose & Merlin L. Bruening. 1999 J. Am. Chem. Soc, 121, 1978-1979
[43] Peter Schuetz & Frank Caruso. 2003 Adv. Funct. Mater, 13, 12, 929-937
[44] Malin Eriksson, Annsofie Torgnysdotter & Lars Wagberg. 2006 Ind. Eng. Chem. Res, 45, 5279-5286
[45] D. M. Sullivan & M. L. Bruening. 2003 Chem. Mater, 15, 281-287
[46] Chen, D., & Zheng, L. Z. 2008 Chinese Journal of Chemistry, 26(2), 276-280.
[47] Kim, B. S., Kim, B., & Suh, K. D. 2008 Journal of Polymer Science Part a-Polymer Chemistry, 46(3), 1058-1065.
[48] Tan, J. P. K., Wang, Q., & Tam, K. C. 2008 Journal of Controlled Release, 128(3), 248-254.
[49] Sleutel, S., De Neve, S., Singier, B., & Hofman, G. 2007 Communications in Soil Science and Plant Analysis, 38(19-20), 2647-2657.
[50] Wright, A. F., & Bailey, J. S. 2001Communications in Soil Science and Plant Analysis, 32(19-20), 3243-3258.
[51] Matejovic, I. 1997 Communications in Soil Science and Plant Analysis, 28(17-18), 1499-1511.
[52] Sieper, H. P., Kupka, H. J., Williams, T., Rossmann, A., Rummel, S., Tanz, N., & Schmidt, H. L. 2006 Rapid Communications in Mass Spectrometry, 20(17), 2521-2527.
[53] Wang, Q. B., Chen, M. J., & Li, Y. C. 2004 Journal of Plant Nutrition, 27(3), 557-569.
[54] Etheridge, R. D., Pesti, G. M., & Foster, E. H. 1998 Animal Feed Science and Technology, 73(1-2), 21-28.
[55] Nzokou, P., & Kamdem, D. P. 2005 Surface and Interface Analysis, 37(8), 689-694.
[56] Sinn, G., Reiterer, A., & Stanzl-Tschegg, S. E. 2001 Journal of Materials Science, 36(19), 4673-4680.
[57] Inari, G. N., Petrissans, M., Lambert, J., Ehrhardt, J. J., & Gerardin, P. 2006 Surface and Interface Analysis, 38(10), 1336-1342.
[58] Tze, W. T. Y., Bernhardt, G., Gardner, D. J., & Christiansen, A. W. 2006 International Journal of Adhesion and Adhesives, 26(7), 550-554.
[59] Johansson LS, Campbell JM, Koljonen K, Stenius P. 1999 Appl. Surf. Sci. 145, 92
[60] W. Gramlich, D. Gardner & D. Neivandt. 2006 J. Adhesion Sci. Technol. 20, 1873-

1887
[61] Wagberg, L., Decher, G., Norgren, M., Lindstrom, T., Ankerfors, M., & Axnas, K. 2008 Langmuir, 24(3), 784-795.
[62] Lu, L. P., Wang, S. Q., & Lin, X. Q. 2004 Analytica Chimica Acta, 519(2), 161-166.
[63] He, P. L., & Hu, N. F. 2004 Electroanalysis, 16(13-14), 1122-1131.
[64] Fujita, S., & Shiratori, S. 2006 Thin Solid Films, 499(1-2), 54-60.
[65] Bertoni, C., Skakalova, V., & Roth, S. 2008 Physica E-Low-Dimensional Systems & Nanostructures, 40(7), 2257-2262
[66] Frank N. Crespilho, Valtencir Zucolotto, Jose R. Siqueira, Carlos J. L. Constantino, Francisco C. 2005Nart and Osvaldo N. Oliveira, Environ. Sci. Technol, 39, 5385-5389
[67] Juan Mendez Garza, Pierre Schaaf, Sylvaine Muller, Vincent Ball, Jean-Francois Stoltz, Jean-Claude Voegel, and Philippe Lavalle, 2004Langmuir, 20, 7298-7302
[68] V. V. Tsukruk, V. N. Bliznyuk, and D. Visser, 1997Macromolecules, 30, 6615-6625
[69] Lvov, Yu. M.; Decher, G. 1994Crystallogr. Rep., 39, 628
[70] Ning Ma, Hongyu Zhang, Bo Song, Zhigang Wang, and Xi Zhang, 2005 Chem. Mater., 17, 5065-5069
[71] Malin Eriksson, Shannon M. Notley, and Lars Wagberg. 2005J. Colloid Interface Sci., 292, 38-45
[72] Paul Podsiadlo, Seok-Youl Choi, Bongsup Shim, Jungwoo Lee, Meghan Cuddihy, and Nicholas A. Kotov, 2005Biomacromolecules, 6, 2914-2918
[73] Kovacevic D, van der Burgh S, de Keizer A, Stuart MAC. 2002 Langmuir, 18, 5607-12
[74] Dubas, S.T.; Schlenoff, J.B. 2001Macromolecules, 34, 3736-3740
[75] Lloyd JA, Horne CW. 1993Nord Pulp Pap Res J, 8, 48-67
[76] Jeeyoung Choi & Michael F. Rubner. 2005 Macromolecules, 38, 116-124
[77] Kamke, F. A., & Lee, J. N. 2007 Wood and Fiber Science, 39(2), 205-220.
[78] Pascal Nzokou & D. Pascal Kamdem, 2005 Surf. Interface Anal, 37, 689-694
[79] Wu, Z. H., Chen, S. P., & Tanaka, H. 2001Journal of Applied Polymer Science, 80(12), 2185-2190.
[80] Wandrey, C., Hernandez-Barajas, J., & Hunkeler, D. 1999 Radical Polymerisation Polyeletrolytes, 145, 123-182.
[81] Sarah L. Clark &Paula T. Hammond. 2000 Langmuir, 16, 10206-10214

[82] Jian Dong, Yukihiro Ozaki & Kenichi Nakashima. 1998 Journal of Polymer Science PartA: Polymer Chemistry, 35, 3, 507-515
[83] Kacurakova, M., Wellner, N., Ebringerova, A., Hromadkova, Z., Wilson, R. H., & Belton, P. S. 1999 Food Hydrocolloids, 13(1), 35-41.
[84] Bertrand P, Jonas A, Laschewsky A and Legras R. 2000 Macromol.Rapid Commun. 21 319-48.
[85] Plech A, Salditt T, Munster C and Peisl J. 2000 J. Colloid Surf. A 190 185-92.
[86] Charles B. Vick, Klaus Richter, Bryan H. River and Albert R.Fried, Jr., 1995 Wood and Fiber Science, 27 (1), 2-22.

APPENDIX

A. Calculation of PEI content on PEI coated wood sample.

$$PEI\% = (N_{coated\text{-}wood}\% - N_{wood}\%) * 3.7$$

B. Calculation of PEI content on PEI(PAA/PAH)$_9$ coated wood samples.

For small early wood wafers, the density of **0.31g/cm3**

Five wood wafers weight around 220mg; thickness of each wafer is 0.15cm

The total **tangential surface area** of **five wafers** is around: $\frac{0.22}{0.31 \times 0.15} \times 2 = 9.46 cm^2$

Because these five wafer weight around 0.22g, and the N content is (0.23-0.05)%. One five wafer there are $0.22 * 0.18\% = 3.96 \times 10^{-4}$ g Nitrogen

The ratio of N to PEI is around 1:3.7. So, when there are 3.96×10^{-4}g N on wood wafers, there are $3.96 \times 10^{-4} * 3.7 = 1.4652 \times 10^{-3}$g PEI on wood

Therefore, there is 1.4652×10^{-3} g PEI on 9.46cm2 wood surface area, which is 1.55×10^{-4} g of PEI per centimeter square of wood.

Wood strips for shear test have the size of 30cm by 6.25cm by 0.9375cm, so the surface area receiving polymer for bonding is 30*6.25=187.5cm2 for each strip.

So, the PEI content on one side of wood strip is $187.5 * 1.55 \times 10^{-4}$ **=0.029g**

C. Calculation of PAH content on PEI(PAA/PAH)$_9$ coated wood samples.

For small early wood wafers, the density of **0.31g/cm3**

Five wood wafers weight around 220mg; thickness of each wafer is 0.15cm

The total **tangential surface area** of **five wafers** is around: $\frac{0.22}{0.31 \times 0.15} \times 2 = 9.46 cm^2$

Because these five wafer weight around 0.22g, and the N content is 0.0345%. One five wafer there are $0.22 * 0.0345\% = 7.58 \times 10^{-5}$ g Nitrogen.

The ratio of N to PAH is around 1:7.14. So when there are 7.58×10^{-5}g N on wood wafers, there are $7.58 \times 10^{-5} * 7.14 = 5.4151 \times 10^{-4}$g PEI on wood

Therefore, there are 5.4151×10^{-4} g PAH on 9.46cm^2 wood surface area, which is 5.7242×10^{-5} g of PAH per centimeter square of wood.

Wood strips for shear test have the size of 30cm by 6.25cm by 0.9375cm, so the surface

area receiving polymer for bonding is 30*6.25=187.5cm2 for each strip.

So one layer of PAH content on one side of wood strip is $187.5 * 5.7242 \times 10^{-5}$**=0.01073g**

Therefore in the multilayer of PEI(PAA/PAH)$_9$ there are 0.01073*9=0.09657g PAH

D. Calculation of PAA content on PEI(PAA/PAH)$_9$ coated wood samples.

The equal amount of PAH for each layer is applied to PAA.